Modellgestützte Entwicklung dielektrischer Elastomer-Aktoren:

Simulation, Aufbau und Validierung intelligenter Antriebslösungen

Dissertation

Zur Erlangung des Grades

des Doktors der Ingenieurwissenschaften

der Naturwissenschaftlich – Technischen Fakultät der

Universität des Saarlandes

von

Matthias Baltes

Saarbrücken

2025

Tag des Kolloquiums:	10.10.2025
Dekan:	Prof. Dr.-Ing. Dirk Bähre
Berichterstatter:	Prof. Dr.-Ing. Paul Motzki Prof. Dr.-Ing. Georg Frey
Akad. Mitglied:	Dr. Michael Roland
Vorsitz:	Prof. Dr.-Ing. Rainer Müller

Tag des Kolloquiums:

Dekan:

Berichterstatter:

Vorsitz:

Akad. Mitarbeiter:

Vorwort und Danksagung

Mit dieser Arbeit endet ein langer Weg, der am Lehrstuhl für Intelligente Materialsysteme (iMSL) nicht nur eine akademische, sondern auch eine persönliche Heimat geworden ist. Vom Bachelorstudium über den Master bis hin zur Promotion habe ich hier nicht nur lernen und forschen können, sondern auch viele gute Menschen kennengelernt, in der Arbeit, aber genauso außerhalb davon. Auch wenn eine Promotion ursprünglich nicht geplant war, hat sich dieser Weg fast automatisch ergeben, vor allem, weil ich den Lehrstuhl nie wirklich verlassen wollte. Die Motivation, an meiner Forschung weiterzuarbeiten, kam immer wieder zurück, mit dem Ziel, irgendwann etwas zu entwickeln, das seinen Platz in einer realen Anwendung findet.

Mein besonderer Dank gilt Stefan Seelecke, Paul Motzki und Gianluca Rizzello, die mich über viele Jahre hinweg ausgebildet, begleitet und betreut haben. Für die Betreuung meiner Abschlussarbeiten und Veröffentlichungen danke ich auch Sophie Nalbach, Philipp Loew und Daniel Bruch. Über die Jahre habe ich viel Input und Unterstützung erhalten, besonders auch in den Phasen, in denen bei der Arbeit mit dielektrischen Elastomeren nicht alles wie geplant funktionierte und Zweifel an der Technologie aufkamen. Mein Dank gilt hier besonders den Kolleginnen und Kollegen aus dem DE-Bereich, die auf unterschiedliche Weise zum Fortschritt beigetragen haben, besonders hervorzuheben Marius Jank während meiner Bachelor- und Masterzeit sowie Sipontina Croce während der Promotion.

Abseits des wissenschaftlichen Arbeitens waren es auch viele andere, die mit dafür gesorgt haben, dass der Alltag nicht zu trocken wurde, sei es durch vieler gemeinsame Pausen, spontane Aktionen oder Aktivitäten nach Feierabend. Ich denke hier weiß jeder Bescheid, der gemeint ist. Insgesamt habe ich die Zeit am iMSL sehr geschätzt, fachlich wie persönlich, und hätte mir für mein Studium und die Promotion keinen passenderen Lehrstuhl wünschen können.

Zusammenfassung

Diese Dissertationsschrift untersucht zwei unterschiedliche Ansätze zur Weiterentwicklung dielektrischer Elastomer-Aktoren (DE-Aktoren) mit dem Ziel, deren Einsatz in realen Anwendungen zu ermöglichen. Im ersten Ansatz wird ein neuartiges Softrobotik-System vorgestellt, das auf einer bistabilen Mechanik basiert und mehrdimensionale, steuerbare Bewegungen erlaubt. Die entwickelte Struktur wurde modellbasiert ausgelegt und experimentell validiert. Der zweite Schwerpunkt liegt auf der Entwicklung einer energieeffizienten, dynamisch angetriebenen Pumpe auf DE-Basis. Der hierfür konzipierte Prototyp erreicht Leistungswerte, die mit konventionellen Technologien vergleichbar sind, und integriert erstmals eine kompakte Elektronik mit Self-Sensing-Funktion zur autonomen Anpassung der Ansteuerfrequenz an den aktuellen Lastdruck. Die Ergebnisse zeigen, dass beide Konzepte wesentliche Fortschritte von der Grundlagenforschung bis hin zu anwendungsnahen Demonstratoren darstellen. Sie legen damit den Grundstein für die zukünftige Integration von DE-Aktoren in funktionale Softrobotik- und Fluidsysteme, die herkömmliche Antriebstechnologien ergänzen oder ersetzen können.

Abstract

This work presents two distinct approaches for advancing dielectric elastomer actuators (DEAs) toward real-world applications. The first focuses on a novel soft robotic system based on a bistable actuator design that enables multidimensional, controllable motion. The structure was developed using a model-based design process and experimentally validated. The second approach centers on the development of an energy-efficient, dynamically driven DEA-based pump. The prototype achieves performance levels comparable to conventional technologies and includes, for the first time, a compact electronics unit featuring self-sensing functionality. This enables autonomous adjustment of the driving frequency in response to the current load pressure. The results demonstrate that both systems represent significant progress, ranging from innovative concepts in fundamental research to application-oriented demonstrators. These developments lay the foundation for the future integration of DEAs into soft robotic and fluidic systems, offering the potential to complement or replace conventional actuation technologies.

Inhaltsverzeichnis

1 Einleitung und Motivation

Elektromechanische Aktuatoren wie Elektromotoren, Verbrennungsmotoren oder Hydraulikzylinder werden in zahlreichen technischen Systemen eingesetzt, von großindustriellen Anlagen bis hin zu Miniaturanwendungen wie Smartphone-Kameras. Neben diesen etablierten Technologien erweitern sogenannte smarte Materialien [1], wie Formgedächtnislegierungen [2], [3], [4], Piezoaktoren [5] und elektroaktive Polymere (EAPs) [6], das Spektrum verfügbarer Antriebslösungen. Sie bieten neuartige Eigenschaften, die sich gezielt nutzen lassen, um Systeme effizienter, kompakter und intelligenter zu gestalten.

Mit dem Fortschritt im Bereich smarter Materialien eröffnet sich die Möglichkeit, bestehende Problemstellungen und technische Aufgabenstellungen, die bisher überwiegend mit klassischen Aktoren gelöst wurden, grundlegend neu zu betrachten. Materialien wie dielektrische Elastomere (DEs) [7], eine Untergruppe der EAPs, erlauben nicht nur eine deutlich leichtere, leisere und formflexible Umsetzung mechanischer Funktionen, sondern ermöglichen durch ihre spezielle elektromechanische Eigenschaften zusätzliche Funktionalitäten wie integrierte Sensorik [8], Zustandsüberwachung und optimierte Effizienzregelung. Zu den EAPs gehören neben DEs auch ionische Polymere [9] und sogenannte HASEL-Aktuatoren [10].

Trotz mehr als 35 Jahren intensiver Forschung ist es DE-Aktoren bisher jedoch nicht gelungen, sich im breiten industriellen Maßstab durchzusetzen. Drei zentrale Herausforderungen bremsen aktuell noch ihren praktischen Durchbruch: die fehlende industrielle Produktionsreife, die begrenzte Leistungsfähigkeit in spezifischen Anwendungen sowie der Bedarf an kompakter, kosteneffizienter Elektronik zur Ansteuerung und Signalauswertung.

Ziel dieser Arbeit ist es, einen Beitrag zur Überwindung dieser Hindernisse zu leisten. Dabei werden zwei komplementäre Ansätze verfolgt, um das Potenzial von DE-Aktoren systematisch zu erschließen. Der erste Ansatz widmet sich neuartigen Anwendungsfeldern, in denen konventionelle Aktoren aufgrund ihrer Starrheit, Größe oder Komplexität an ihre Grenzen stoßen, insbesondere im Bereich der Soft-Robotik. Der zweite Ansatz zielt darauf ab, DE-Aktoren in direkte Konkurrenz zu bestehenden Technologien zu setzen. Ein konkretes Beispiel für diese Zielsetzung ist die Entwicklung einer Pumpenanwendung, bei der dielektrische Elastomer-Aktoren nicht nur eine vergleichbare Leistung wie konventionelle Pumpen erreichen sollen, sondern durch ihre besonderen Materialeigenschaften eine smartere und überlegene Lösung darstellen können. Ziel ist es, ein System zu schaffen, das neben hoher Leistungsdichte und Effizienz auch integrierte Sensorfunktionen [8], [11], [12], [13], schnelle Reaktionszeiten und eine kompakte Bauweise ermöglicht. Eigenschaften, die mit klassischen Technologien nur schwer oder gar nicht realisierbar sind.

Im folgenden Abschnitt werden zunächst die grundlegenden physikalischen und materialtechnischen Eigenschaften dielektrischer Elastomere erläutert. Daran anschließend erfolgt eine Darstellung des aktuellen Stands der Technik in den für diese Arbeit relevanten Anwendungsbereichen. Auf dieser Basis werden schließlich die zentralen Forschungsfragen abgeleitet, die im Rahmen der vorliegenden Dissertation untersucht werden.

1.1 Grundlagen

Im Zentrum dieser Arbeit stehen DEs. Charakteristisch für DEs ist die Umwandlung elektrischer Energie in mechanische Arbeit auf Grundlage elektrostatischer Kräfte.

Ein typischer DE besteht aus einem dünnen, elastischen Polymerfilm, der beidseitig mit flexiblen, leitfähigen Elektroden beschichtet ist.

Für den Polymerfilm kommen verschiedene Materialien zum Einsatz, darunter Silikone (z. B. Elastosil 2030), acrylische Polymere (z. B. VHB) und Naturkautschuk [14], [15], [16]. Diese unterscheiden sich hinsichtlich ihrer maximalen Dehnung, Reaktionszeit, Verarbeitungseigenschaften und Alterungsbeständigkeit. VHB-Folien ermöglichen sehr hohe Dehnungen von bis zu 400–500 %, reagieren jedoch relativ träge [15], [16]. Silikon hingegen erreicht geringere Dehnungen von etwa 100 %, weist dafür aber eine um ein Vielfaches schnellere Reaktionszeit auf [15], was es besonders für dynamische Anwendungen attraktiv macht.

Die Elektroden werden typischerweise aus Carbon-Black-Silikon-Gemischen [11], Kohlenstoffnanoröhren [17] oder gesputterten Metallfilmen hergestellt [18], [19]. Die Wahl des Elektrodenmaterials beeinflusst vor allem den elektrischen Widerstand sowie die Flexibilität des gesamten Verbundes [17]. Eine sorgfältige Abstimmung von Polymerfilm und Elektrodenmaterial ist entscheidend für die Leistungsfähigkeit und Lebensdauer eines DE-Aktors [15].

Funktional entspricht dieser Aufbau einem flexiblen Plattenkondensator, bei dem sowohl das Dielektrikum als auch die Elektroden mechanisch verformbar sind [8], [20]. Wird eine Hochspannung an die Elektroden angelegt, entsteht ein elektrisches Feld E innerhalb der Struktur, das elektrostatische Anziehungskräfte zwischen den Elektroden erzeugt [20]. Die entstehende Druckkraft wird als Elektrostatische Druck (bzw. Maxwell Stress) p bezeichnet, wobei ε_0 die elektrische Feldkonstante und ε_r die relative Permittivität des Dielektrikums ist.

Maxwell Stress: $$p = \frac{1}{2}\,\varepsilon_0 \varepsilon_r E^2$$ Formel 1

Diese Kräfte komprimieren den Polymerfilm in Dickenrichtung, während sich dieser aufgrund seiner nahezu inkompressiblen Eigenschaften gleichzeitig in der Fläche ausdehnt. Dieser Dehnungsprozess kann zum Erzeugen einer gezielten mechanischen

Bewegung genutzt werden. Im Gegensatz dazu kann der DE auch als Sensor eingesetzt werden, indem seine kapazitiven Änderungen bei mechanischer Verformung gemessen werden [8]. Die Kapazität C eines DEs ist dabei von der Fläche A der Elektroden und der Dicke d des Dielektrikums abhängig und wird durch die Formel 2 beschrieben.

Kapazität Plattenkondensator: $$C = \varepsilon_0 \varepsilon_r \frac{A}{d}$$ Formel 2

Da die Kapazität abgesehen von den Material-/Feldkonstanten nur von den Geometrieparametern des DEs abhängt, eignet sich diese Kenngröße gut als Sensor für Flächenänderungen. Wird die Kapazität während der Aktorbewegung überwacht, kann der DE-Aktor seine Position selbst erfassen, ohne einen externen Sensor zu benötigen. Dieser Mechanismus wird als Self-Sensing-Effekt bezeichnet [12], [13], [21].

Sowohl die Flächenvergrößerung als auch die Dickenverringerung des Polymerfilms sind wesentliche Effekte, die in Aktorsystemen gezielt eingesetzt werden können, um mechanische Bewegungen zu erzeugen oder Kräfte zu übertragen.

Die Dicke eines DE-Films liegt typischerweise im Bereich von wenigen zehn Mikrometern, etwa zwischen 20 µm und 80 µm, und ist im Vergleich zur möglichen Flächenausdehnung deutlich kleiner. Dieser geringe Dickenmaßstab ist notwendig, um ein ausreichend starkes elektrisches Feld aufzubauen, da die Feldstärke E direkt von der angelegten Spannung U und der Dicke d des Films abhängt.

Elektrische Feldstärke: $$E = \frac{U}{d}$$ Formel 3

Um eine nennenswerte Verformung zu erzielen, sind trotz der dünnen Schicht sehr hohe elektrische Spannungen von bis zu mehreren tausend Volt erforderlich. Aufgrund dieser Abhängigkeit kann die Dicke nicht ohne weiteres vergrößert werden, da eine dickere Schicht eine proportional höhere Spannung erfordern würde, um das gleiche Feld zu erzeugen (Formel 3) .

Die Dickenveränderung eines einzelnen DE-Films ist daher mechanisch nur gering und begrenzt die Hubhöhe des Aktors. Um größere Bewegungsamplituden zu erreichen, können mehrere DE-Filme übereinander gestapelt werden. Durch diese Stapelung addieren sich die einzelnen Dickenänderungen der Schichten über die Superposition, sodass sich der Gesamthub proportional erhöht [22]. Ein wesentlicher Vorteil dieses Stapel-Aktoren-Prinzips besteht darin, dass es ohne den Einsatz von zusätzlichen Vorspannelementen auskommt.

Im Gegensatz dazu wird bei der Flächenvergrößerung, abhängig vom verwendeten Material, eine deutlich größere Verformung ermöglicht, die im Bereich von 100 bis 400 % der Ausgangsgröße liegen kann. Um diese großen Dehnungen gezielt nutzbar zu machen, muss der Film jedoch mit einem Vorspannelement kombiniert und konstant unter mechanischer Spannung gehalten werden. Durch das Vorspannelement wird der DE-Film gezielt in die Länge gezogen und bleibt straff, sodass ein Durchhängen vermieden wird.

Die maximale Bewegung des DEs lässt sich hierbei über die Flächengeometrie und die Wahl des Vorspannelements skalieren. Die erzeugbare Kraft kann hingegen durch das Stapeln mehrerer DE-Schichten übereinander nach dem Superpositionsprinzip erhöht werden, wobei die Kraft auch vom Arbeitspunkt beeinflusst wird, der durch das Vorspannelement und die mechanische Last definiert wird [23].

Für die Wahl des Vorspannmechanismus steht eine breite Palette an Optionen zur Verfügung, die von einer konstanten Masse über lineare Federn (Linear Bias Springs, LBS), Federn mit negativer Steifigkeit (Negative Bias Springs, NBS) [24], Permanentmagneten [25] bis hin zu weiteren komplexen Mechanismen reicht [26], [27]. Je nach Anwendung kann das passende Vorspannelement ausgewählt werden .

1.2 Stand der Technik

Der einfachste Fall zur Auslegung eines dielektrischen Elastomer-(DE-)Aktors ist die Betrachtung eindimensionaler, statischer Bewegungen. In diesem Szenario lässt sich die Kraft-Weg-Charakteristik eines DE-Elements durch einfache Charakterisierung oder Modellierung bestimmen. Anhand dieser Kennlinie sowie der grafischen Analyse des statischen Gleichgewichts zwischen dem aktivierten beziehungsweise nicht aktivierten DE-Element und dem Vorspannelement können maximaler Hub, Blockierkräfte sowie die Aktorkennlinie direkt abgeleitet werden [20], [28], [29]. Diese lässt sich durch gezieltes Design des DE-Elements und des Vorspannelements an die jeweilige Anwendung und die geforderte Last anpassen.

Ein exemplarisches Anwendungsfeld für diesen Fall sind Ventilsysteme [30], [31], [32], [33], bei denen die Bewegungen typischerweise eindimensional mit begrenztem Hub erfolgen und die Ventile häufig quasi-statisch betrieben werden. Aufgrund der vergleichsweise einfachen Bewegungsanforderungen ist die Auslegung von DE-Aktoren in solchen Anwendungen gut realisierbar, was durch zahlreiche experimentelle Studien bestätigt wird [30], [31], [32], [33]. Allerdings ist der Wettbewerb in diesem Bereich hoch. Etablierte Technologien wie elektromagnetische Ventile oder Ventile mit piezoelektrische Aktoren sind kosteneffizient, ausgereift und in großen Stückzahlen verfügbar. Dennoch bieten DE-Aktoren spezifische Vorteile, etwa die Möglichkeit, Positionen nahezu ohne Energiezufuhr zu halten. Zusätzlich ermöglicht der Self-Sensing-Effekt eine integrierte Zustandsüberwachung ohne externe Sensorik, was die Systemintegration vereinfacht und potenzielle Kosten senkt.

Trotz dieser Vorteile stehen DE-Aktoren vor wesentlichen Herausforderungen, die ihre breite Anwendung in der Massenproduktion bislang verhindern. Der erste offene Forschungspunkt betrifft daher die Fertigung: Diese muss standardisiert, automatisiert und qualitativ hochwertig gestaltet werden, um sowohl Dauerfestigkeit als auch geringe Ausschussraten zu gewährleisten. Darüber hinaus ist eine speziell auf DE-Aktoren zugeschnittene, kompakte und effiziente Elektronik erforderlich, die sowohl die präzise Ansteuerung als auch die Auswertung der Self-Sensing-Signale ermöglicht.

Komplexere Bewegungsprofile, wie sie in mehrdimensionalen oder dynamischen Systemen auftreten, können durch die einfache, statische Auslegung nicht adäquat beschrieben oder realisiert werden. Solche Anforderungen finden sich insbesondere in der Soft-Robotik, einem Bereich, der durch flexible und adaptive Strukturen gekennzeichnet ist und in dem herkömmliche Aktoren häufig keine optimale Lösung darstellen.

Vor diesem Hintergrund wird in der Soft-Robotik intensiv an smarten Materialien geforscht, die direkt in flexible, weiche Strukturen integriert werden können. Beispiele hierfür sind Formgedächtnislegierungen [34], ionische Polymer-Metall-Komposite [35] sowie weitere intelligente Werkstoffe. Zusätzlich kommen häufig pneumatische und hydraulische Systeme zum Einsatz, bei denen Fluide in weiche Strukturen gepumpt werden, die sich dadurch bewegen oder biegen [36], [37]. Diese Systeme sind jedoch meist auf externe Pumpen, Kompressoren und Ventile angewiesen, was die Integration in kompakte und autonome Systeme erschwert.

Die Integration von smarten Materialien wie DEs bietet neue Möglichkeiten, flexible Systeme direkt mit integrierten Aktoren auszustatten und so die Soft-Robotik nachhaltig weiterzuentwickeln. Zwar existieren bereits verschiedene Ansätze mit DEs, häufig wird jedoch das Material VHB eingesetzt, das aufgrund seiner langsamen Ansprechzeit nur begrenzte Bewegungsgeschwindigkeiten ermöglicht [38], [39], [40], [41], [42], [43]. Hierbei ergibt sich der nächste Forschungsschwerpunkt: Während Silikon aufgrund seiner schnellen Reaktionsfähigkeit bereits vereinzelt in der Soft-Robotik eingesetzt wird, ist bislang unklar, ob und wie das Konzept bistabiler Systeme, das sich für eindimensionale Bewegungen bewährt hat, auf mehrdimensionale Strukturen übertragen und entsprechend angepasst werden kann.

Neben den zuvor betrachteten statischen, eindimensionalen sowie mehrdimensionalen Bewegungen stellt die Realisierung dynamischer Bewegungen ein weiteres wichtiges Einsatzfeld für dielektrische Elastomer-Aktoren dar. Hierzu zählen Anwendungen wie Lautsprecher [44], [45], haptische Feedbacksysteme [46] sowie insbesondere Pumpensysteme, in denen schnelle, wiederholte Bewegungsabläufe erforderlich sind. In diesen Bereichen existieren bereits zahlreiche Demonstratoren und Prototypen [47], [48], [49], [50], [51], [52], [53], [54], [55], die die prinzipielle Eignung von DE-Aktoren belegen.

Insbesondere bei Pumpen, die in vielfältigen technischen Systemen eingesetzt werden, steht man jedoch in direkter Konkurrenz zu etablierten konventionellen Technologien. Um hier konkurrenzfähig zu sein, ist es zwingend erforderlich, vergleichbare Leistungsbereiche, etwa in Bezug auf Fördermenge, Druckaufbau und Effizienz zu erreichen. Genau an diesem Punkt zeigen sich jedoch die zentralen Herausforderungen für DE-basierte dynamische Aktoren: Es reicht nicht aus, lediglich einzelne Komponenten zu entwickeln. Vielmehr muss das gesamte System, bestehend aus Aktor, Mechanik und Ansteuerung als Einheit verstanden, modelliert und optimiert werden.

Ein entscheidender Forschungsschwerpunkt liegt daher in der modellbasierten Auslegung und Simulation solcher Systeme, mit dem Ziel, die Effizienz und Leistungsfähigkeit so zu steigern, dass DE-Pumpen funktional mit konventionellen Lösungen konkurrieren können. Gelingt dies, können dielektrische Elastomer-Aktoren nicht nur durch ihre kompakte Bauweise und Integration in weiche Strukturen punkten, sondern auch durch zusätzliche Vorteile wie geringes Gewicht, Self-Sensing und potenzielle Energieeinsparungen im Betrieb.

Die sich aus dem dargestellten Stand der Technik ableitenden Forschungsschwerpunkte werden im folgenden Abschnitt gezielt formuliert und zusammengefasst.

1.3 Forschungsfragen

Übergeordnete Leitfrage (Rahmen der Dissertation):

1. *Inwiefern können dielektrische Elastomer-Aktoren (DE-Aktoren) durch intelligente Auslegung, Fortschritte in der Herstellung, Design und Systemintegration weiterentwickelt werden, dass sie eine realistische, wettbewerbsfähige Alternative zu etablierten Aktorsystemen darstellen?*

Material & Herstellung (Grundlage für alle Anwendungen):

2. *Kann der Herstellungsprozess von DE-Aktoren mit Hinblick auf reproduzierbare Qualität, hohe Dauerfestigkeit und Skalierbarkeit für die Massenproduktion weiterentwickelt werden?*

Mehrdimensionale Bewegungen (Soft-Robotik):

3. *Inwieweit lassen sich bistabile Konzepte, die bisher für eindimensionale DE-Aktoren genutzt wurden, auf mehrdimensionale Systeme übertragen, um große Hübe zu realisieren?*
4. *Können Silikon-basierte DE-Aktoren Aktorhübe erreichen, die mit VHB-basierten Systemen vergleichbar sind und gleichzeitig verbesserte Reaktionszeiten in Soft-Robotik-Strukturen realisieren?*

Dynamische Bewegungen (Pumpen):

5. *Lassen sich Antriebssysteme auf DE-Aktor Basis in Leistungsdichte und Antriebsleistung entwickeln um konventionelle Pumpenantriebe zu ersetzen?*

6. *Wie kann das Gesamtsystem, bestehend aus DE-Aktor, Pumpenstruktur und Last, modellbasiert und simulationsgestützt so ausgelegt werden, dass die Energieeffizienz maximiert und die Betriebsweise optimiert wird?*
7. *Wie kann der Self-Sensing-Effekt von DEs in Verbindung mit kompakter, kosteneffizienter Elektronik genutzt werden, um relevante Systemkenngrößen (z. B. Druck, Auslenkung) präzise zu erfassen und zu überwachen?*
8. *In welchem Maße lässt sich durch die Integration von Self-Sensing und intelligenter Ansteuerungselektronik ein autonomes, adaptives Pumpensystem realisieren, das herkömmlichen Pumpen überlegen ist?*

2 Publikationen zum modellbasierten Design mehrdimensionaler und dynamischer Aktorsysteme auf Basis dielektrischer Elastomere

In diesem Abschnitt werden drei wissenschaftliche Arbeiten vorgestellt, die sich unmittelbar mit der in der Motivation beschriebenen Herausforderung befassen: der systematischen Entwicklung eines funktionalen Gesamtsystems auf Basis dielektrischer Elastomer-Aktoren mit dem Ziel, deren Einsatz in praxisnahen Anwendungen zu ermöglichen.

Dabei greifen die Arbeiten die zentralen Forschungsfragen dieser Dissertation auf. Sie setzen sich zunächst mit der Frage auseinander, wie DE-Aktoren so gestaltet und gefertigt werden können, dass sie sowohl für den experimentellen Aufbau als auch perspektivisch für eine massenproduktionstaugliche Nutzung geeignet sind. Darauf aufbauend adressieren die Arbeiten, wie sich bekannte Funktionsprinzipien, wie etwa bistabile Konzepte zur Hubvergrößerung, gezielt auslegen und auf mehrdimensionale Anwendungsbereiche, wie Softrobotik übertragen lassen.

Allen drei Beiträgen liegt ein einheitlicher, modellbasierter Entwicklungsansatz zugrunde: Ausgehend von der modellgestützten Beschreibung und Simulation des elektromechanischen Verhaltens der Aktoren bis hin zur Integration in konkrete Anwendungsszenarien unter Berücksichtigung aller relevanten Systemkomponenten. Die einzelnen Arbeiten verdeutlichen dabei die gesamte Entwicklungskette, von Design und Herstellung über Optimierung und Validierung bis hin zur Entwicklung funktionaler Prototypen.

Durch diese strukturierte Herangehensweise wird deutlich, wie die Kombination aus präziser Modellbildung, experimenteller Validierung und systemischer Optimierung dazu beitragen kann, die Einsatzfähigkeit von DE-Aktoren über das Laborniveau hinaus in reale technische Anwendungen zu überführen.

2.1 Zusammenfassung der Publikationen

Die erste Publikation beschäftigt sich mit der Entwicklung eines Softrobotik-Moduls, das speziell für mehrdimensionale Bewegungen konzipiert ist. Softrobotiksysteme orientieren sich häufig an Vorbildern aus der Natur, insbesondere an den Bewegungsmechanismen biologischer Muskulatur. In dieser Arbeit wird dieses Prinzip durch den Einsatz sogenannter Rolled Dielectric Elastomer Actuators (RDEAs) aufgegriffen. Diese gerollten DE-Aktoren funktionieren ähnlich wie Muskelfasern: Sie lassen sich bündeln, um die Kraft zu skalieren, und verändern ihre Länge beim Anlegen einer Hochspannung.

Das zentrale Konzept basiert auf dem bistabilen Vorspannelement, einem aus der eindimensionalen Aktorik bekannten Prinzip, welches hier auf eine mehrdimensionale Struktur übertragen wird. Während bisherige DE-basierte Softrobotiksysteme mit Silikon meist nur geringe Biegewinkel von unter 10° erreichen, und VHB-basierte Ansätze zwar größere Biegewinkel, jedoch nur langsame Bewegungen ermöglichen, realisiert die vorliegende Arbeit eine schnelle, große und kontrollierbare Bewegung durch die Verwendung einer bistabilen Mechanik.

Die entwickelte Struktur, in der Publikation als „T-Plattform" bezeichnet, besteht aus zwei RDEAs, die zwischen einer Grundplatte und einer beweglichen Plattform montiert sind. Zentral zwischen den DEs wird ein elastischer Balken montier. Dieser spannt die DEs vor und wird dementsprechend durch eine Druckkraft belastet. Durch diese Kraft knickt der Balken gezielt in eine Richtung ab, was zu einer Auslenkung der Plattform führt. Die Geometrie ist so ausgelegt, dass die Plattform zwei stabile Zustände hat. Eine gezielte Ansteuerung der DEs ermöglicht das kontrollierte Umschalten zwischen diesen Positionen, wodurch ein bistabiles, mehrdimensionales Bewegungssystem entsteht.

Die DE-Geometrien sowie die des Balken werden mithilfe eines Modells entworfen, um die gewünschte bistabile Struktur zu erreichen. Parameter wie Länge, Durchmesser und Vorspannung der Aktoren sind auf das mechanische Verhalten des Balkens abgestimmt. In einem iterativen Prozess wird das Modell durch experimentelle Untersuchungen und Variation zentraler Einflussgrößen, beispielsweise der Montagepunkte, Balkengeometrie und Plattformabmessungen, kontinuierlich optimiert.

Das entwickelte Softrobotikmodul erreicht somit einen Auslenkungswinkel von über 25° in beide Richtungen und demonstriert damit erfolgreich die Machbarkeit eines mehrdimensionalen, DE-basierten, bistabilen Systems.

Die zweite Publikation widmet sich, im Gegensatz zur ersten, die auf quasi-statische, mehrdimensionale Bewegungen fokussiert, einem System für dynamische, eindimensionale Bewegungen unter variabler Last. Ziel ist die Entwicklung eines leistungsstarken Pumpensystems auf Basis von DE-Aktoren.

Im Designprozess erfolgt zunächst eine Analyse geeigneter Pumpmechanismen und passender DE-Aktorkonzepte. Auf dieser Basis wird das Gesamtsystem parametrisiert und modelliert. Für ein effizientes Design fließen sämtliche relevanten Eigenschaften ein, mechanische Parameter aller Komponenten, deren lastabhängiges Verhalten, etwa die Schaltpunkte von Ventilen, sowie die Charakteristika der zu erwartenden Lasten.

Das resultierende Systemmodell wird simulativ untersucht, und die Parameter werden gezielt auf die gewünschte Zielstellung hin angepasst. In diesem Fall handelt es sich um eine Vakuumpumpe mit einem angestrebten Durchfluss von 0,5 L/min bei einer maximalen Druckdifferenz von 700 mbar, entsprechend einem absoluten Druck von 300 mbar. Um die Pumpe leistungsstark zu gestalten, wird die gewünschte Arbeitsfrequenz mit der Eigenresonanz des Systems synchronisiert. Das Modell wird dazu durch iterative Entwicklung der einzelnen Komponenten validiert und optimiert.

Ein besonderer Schwerpunkt liegt auf Robustheit und Langlebigkeit. Alle Bauteile sind mit Sicherheitsfaktoren ausgelegt. Zudem entsteht ein neuer Herstellungsprozess für die Aktoren, der für eine potenzielle Massenproduktion geeignet ist. Das Ergebnis sind kompakte und leistungsstarke Aktorelemente, die Blockierkräfte über 2 N und Hübe bis 10 mm generieren, bei einem Bauraum von nur 45 mm x 45 mm x 4 mm.

Im finalen Schritt dieser Publikation wird die Pumpe aufgebaut und experimentell mit den Zielwerten validiert. Der Vergleich mit dem Stand der Technik zeigt, das System gehört zu den ersten leistungsstarken DE-basierten Pumpen, die signifikante Kräfte erzeugen und mechanische Arbeit verrichten, bei einem kompakten Bauraum.

Die dritte Publikation greift eine zentrale Erkenntnis aus der zweiten Arbeit auf, die Resonanzfrequenz der Pumpe verschiebt sich in Abhängigkeit von der Last, also der Differenz zwischen Umgebungsdruck und erzeugtem Vakuum. Ziel ist es nun, das System so zu betreiben, dass es sich stets im optimalen Frequenzbereich bewegt, und damit maximal energieeffizient arbeitet.

Im ersten Schritt erfolgt die Identifikation der druckabhängigen Resonanzfrequenz mithilfe externer Sensorik. Aufbauend auf dieser Messung wird die Ansteuerfrequenz dynamisch angepasst, um das System kontinuierlich im optimalen Betriebsbereich zu halten.
Im nächsten Schritt soll der sogenannte Self-Sensing-Effekt der DEs genutzt werden, um auf externe Sensorik verzichten zu können. Analysiert wird, wie sich elektrische Signale, insbesondere Entladestrom, in Abhängigkeit von Druck und Frequenz verändern. Modell und Messungen liefern den maximalen Hub, der sich mit dem Entladestrom rekonstruieren lässt, daraus lässt sich die Druckdifferenz ableiten. Diese wird wiederum zur Frequenzregelung herangezogen.

Abschließend entsteht eine kompakte, eigens entwickelte Elektronik, die alle Funktionen integriert, Ansteuerung der Pumpe mit Hochspannung, Self-Sensing über Strommessung beim Entladen, sowie die adaptive Frequenzregelung in Echtzeit.

Diese Optimierung steigert die Effizienz des Gesamtsystems im Vergleich zur zweiten Veröffentlichung um weitere 30 Prozent. Damit entsteht ein vollständig durchentwickeltes System, von der Aktorentwicklung über Modellierung und Simulation bis hin zur intelligenten Regelung und Elektronik, einsatzbereit für reale Anwendungen.

2.2 A bi-stable soft robotic bendable module driven by silicone dielectric elastomer actuators: design, characterization, and parameter study

Hinweis zur Veröffentlichung:
Dieses Kapitel basiert auf folgendem begutachteten und zur Publikation angenommenen Artikel:

Autor(en): Matthias Baltes[1], Julian Kunze[1], Johannes Prechtl[1], Stefan Seelecke[1] and Gianluca Rizzello[1]

[1] M. Baltes, J. Kunze, J. Prechtl, S. Seelecke, and G. Rizzello are with the Department of Systems Engineering and the Department of Material Science and Engineering, Saarland University, Saarbrücken 66123, Germany (phone: +49 (0)681-302-71357; e-mail: {matthias.baltes, julian.kunze, johannes.prechtl, stefan.seelecke, gianluca.rizzello}@imsl.uni-saarland.de)

Titel: A bi-stable soft robotic bendable module driven by silicone dielectric elastomer actuators: design, characterization, and parameter study

Journal: *Smart Materials and Structures*, IOP Publishing

DOI: https://doi.org/ 10.1088/1361-665X/ac96df

Hinweis:

A bi-stable soft robotic bendable module driven by silicone dielectric elastomer actuators: design, characterization, and parameter study

Matthias Baltes[1], Julian Kunze[1], Johannes Prechtl[1], Stefan Seelecke[1] and Gianluca Rizzello[1]

[1] M. Baltes, J. Kunze, J. Prechtl, S. Seelecke, and G. Rizzello are with the Department of Systems Engineering and the Department of Material Science and Engineering, Saarland University, Saarbrücken 66123, Germany (phone: +49 (0)681-302-71357; e-mail: {matthias.baltes, julian.kunze, johannes.prechtl, stefan.seelecke, gianluca.rizzello}@imsl.uni-saarland.de)

E-mail: matthias.baltes@imsl.uni-saarland.de

Received 1 July 22, revised 19 September 2022
Accepted for publication 30 September 2022
Published 17 October 2022

Abstract

In this paper, we present a novel concept for a planar soft robotic module actuated by smart artificial muscles. The structure consists of a flexible backbone capable of continuously bending along a plane, and having a rigid plate connected to its top. The actuation is provided by an antagonist-agonist pair of artificial muscle fibers, consisting of silicone-based rolled dielectric elastomer actuator (RDEA) membranes connected to the rigid top plate. When actuated via high voltage, the RDEAs expand and, in turn, cause the structure to bend along a desired direction. The novel prototype concept is described in detail first, and systematic parameter studies are conducted afterwards by means of a physics-based model. Then, an experimental prototype is manufactured and tested, with the aim of validating the dependency of the bending angle performance on the system design parameters. We demonstrate that the bending angle is strongly affected by the choice of the flexible beam geometry, as well as the RDEAs mounting points. It is found that, for some combinations of parameters, the buckling instability of the beam can be suitably triggered by the RDEAs, resulting in large bending angles up to 25°. This feature also allows to keep the robot deformed without supplying any electric power. In contrast, parameters corresponding to mono-stable configurations result in a maximum bending angle of 11° only.

Keywords: dielectric elastomer, dielectric elastomer actuator, soft robotics, bi-stability, bendable module, characterization

1. Introduction

Conventional industrial robots, typically consisting of solid metal structures controlled by heavy and bulky drive systems, require special safety measures when employed in human-robot collaboration paradigms [1]. Those measures include sensitive artificial skins, which make use of capacitive sensors to detect humans and obstacles prior to collision [2], or limitations imposed to the maximum payloads and velocity [3]. These solutions, however, result in an unavoidable increase in implementation effort and costs. The field of soft robotics offers an alternative way to address this issue. Thanks to their structural compliance and high flexibility, soft robots allow to intrinsically reduce potential harms to the user [4].

In order to effectively control the large number of degrees of freedom (DoF) of soft robots without affecting their flexibility and compliance, suitable actuator solutions are required. Up to date, the most common driving technologies used in soft robotics are based on pneumatics [5], [6] and motor-driven tendons [7], [8]. Despite effectively providing actuation to the soft robot without affecting its structural stiffness, those solutions rely on bulky and heavy components (e.g., compressors, motors, transmissions) which unavoidably affect the overall system weight, size, and efficiency.

It has been remarked how smart material transducers represent a highly promising alternative for embedding actuation into soft robots [9]. Because of their high flexibility and lightweight, smart materials can be directly integrated within the soft robot structure without requiring additional bulky driving units and mechanical transmissions. Among the many types of smart materials, dielectric elastomers (DEs) appear among the most promising ones for robotic and mechatronic applications [10]. A DE consists of a thin elastomer film (e.g., silicone, acrylic, natural rubber) surrounded by compliant electrodes, which undergoes a surface expansion when subject to high voltage. DEs are often referred to as artificial muscles, because of their large deformation, flexible design, high energy density and efficiency, fast response time, silent operation, and possibility to work as actuators and sensors at the same time (self-sensing) [11], [12], [13]. DE actuators (DEAs) can be directly integrated within the structure of a soft robotic system without negatively affecting the overall compliance, weight, and energy efficiency [10]. Several examples of DE soft robot prototypes have been recently proposed in the scientific literature, including soft grippers [14], flexible trunks [15], [16], crawling robots [17], and swimming robots [18], [19]. Most of current works on DE soft robots focus on developing novel concepts to integrate the actuation principle of DEAs within multi-DoF structures. It is worthwhile mentioning that the vast majority of DE soft robot prototypes presented in the literature make use of acrylic material like VHB™ 4910 as elastomer [10], [20]. What makes this material attractive for soft robotic applications is the large strain (up to 400-500%), together with the relatively low elastic modulus (on the order to 20 kPa [21]). These features allowed researchers to design bending actuators with a deflection angle larger than 90° [23]. Despite their advantages, acrylic DEs suffer from some limitations such as high electro-mechanical losses, high response time, sensitivity to environmental conditions, scarce reliability, and lack of scalable manufacturing process (e.g., for the integration of compliant electrodes) [21], [22]. In contrast, silicone (i.e., PDMS)-based DEs are characterized by lower mechanical losses, fast response time (50 times faster [24]) lower leakage conductivity, and longer (>100 times [25]) cyclic lifetime than acrylics, even though they can undergo smaller deformations (on the order of 100% [26]). In addition, scalable and systematic processes have been developed to manufacture compliant electrodes on silicone DE membranes, such as screen printing [27] or spray coating [28]. All those characteristics make silicone a more efficient and reliable material for DE applications [24]. Despite the remarkable advantages of silicone DE, at present there is still a lack of approaches for soft robotic concepts based on this material in the scientific literature. One of the very few examples is the work in [29], in which a silicone-based DE gripper was proposed capable of bending angles up to 60°. In our earlier paper [30], we developed a rotational soft robot concept driven by a double-cone silicone DEA. In this work, the relationship between geometric parameters on the resulting bending angle was systematically investigated, and used to develop design rules which allowed to increase the bending angle almost fivefold, from an initial 2.2° up to 9.6°. From the last example, it is clear how model-based design optimization is essential to exploit the potential of silicone-based DE robotic systems, since it may offer a means to overcome the shortcomings of the material in comparison to acrylic (mostly in terms of strain range) while keeping all its other advantages. Up to date, however, there is a substantial lack of works which perform systematic investigations aimed at developing proper system understanding, design rules for performance scaling, as well as self-sensing based position control architectures for DE soft robots. This is possibly due to the increased level of complexity in comparison to the simpler (and much more understood) case of single-DoF DEAs. Indeed, our previous paper [30] represents one of the first works presenting such type of investigation in the context of DE-based robotic systems. Another crucial aspect for design optimization concerns the use of negative stiffness biasing elements in combination with the DEAs, to increase the achievable motion range. This concept has been extensively used for single-DoF DEA configurations, where a suitable negative stiffness behavior can be implemented based on pre-compressed metal beams [31], or via attracting permanent magnets [32]. Up to date, however, there is still a lack of understanding on how to extend this concept to multi-DoF DE systems such as robots, for which the graphical design methods commonly used in the single-DoF case can no longer be applied.

With the aim of developing and systematically analyzing innovative soft robotic concepts based on DE technology, in this paper we present a novel bendable module driven by silicone-based rolled DE membranes. The first concept of such a system was initially introduced in [33], where only simulation studies were conducted without providing any experimental realization and validation. The system, hereafter referred to as T-platform, consists of a flexible beam capable of bending in-plane, whose tip is connected to a rigid plate. Two pre-tensioned silicone-based rolled DEA (RDEA) elements are mounted on the top plate, acting as an agonist-antagonist pair of artificial muscle fibers [34]. When a RDEA is actuated via high voltage, it expands along its main axis and causes the structure to bend on the opposite direction. Many of those bendable modules can be connected in series, and used to develop a flexible tentacle arm. To begin with, we describe the operating principle of the T-platform, and discuss the most suitable set of parameters which can be studied to optimize its design. Afterwards, we present an extensive model-based parameter study of the T-platform, aimed at understanding how the system free parameters (beam geometry, RDEAs mounting points) affect the resulting bending angle upon electrical actuation. Such a study allows us to determine suitable combinations of design parameters, which are then verified experimentally by means of an extensive characterization campaign. To this end, a novel concept is proposed for the first practical realization and manufacturing of the T-platform prototype. It is found that, for some combinations of design parameters, the buckling instability of the beam can be suitably triggered by the

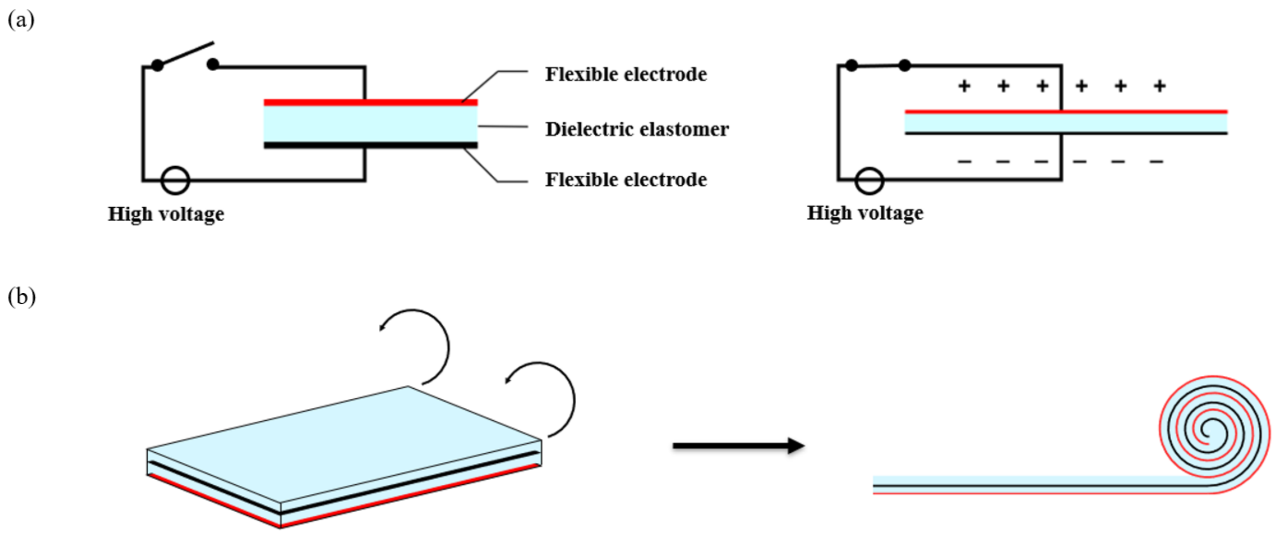

Figure 1: Working principle of DEAs: (a) SIP-DEA, (b) RDEA.

RDEAs, resulting in bending angles up to 25°. This is higher by a factor of 2.5 compared to our previous bendable module concept based on double-cone silicone DEAs [30], for which a maximum bending angle of 9.6° was achieved. Furthermore, compared to the double-cone design in [30], the T-platform is also more suitable for up-scaling and stacking due to its improved aspect ratio. The possibility of exploiting the beam buckling instability to increase the bending angle was initially discovered and analyzed in [35], but the concept was never validated experimentally. The present work represents, to the best of our knowledge, the first experimental validation of a RDEA-driven T-platform, in which a bi-stability-induced magnification of the motion range is demonstrated for the first time in multi-DoF DE soft robots. In addition, this work validates for the first time the ability of the T-platform model initially priposed in [35] to describe a large number of experimental design geometries.

The remainder of this paper is organized as follows. In Section 2, the RDEAs are described. The novel T-platform is then discussed in Section 3, alongside with a model-based study aimed at understanding how the free design parameters affect the system actuation performance. The T-platform manufacturing process is described in Section 4, while the experimental validation of the model-based parameter study is then presented in Section 5. Finally, concluding remarks are discussed in Section 6.

2. Rolled Dielectric Elastomer Actuators

The operating principle of the RDEAs used in this work is briefly summarized in this section. For more details on RDEAs design and manufacturing, the reader may refer to [34].

2.1. Working principle of DEs

The basic structure of a DE corresponds to the one of a parallel-plate capacitor with flexible electrodes and dielectric [36]. By applying high voltage to the electrodes, attractive Coulomb forces are generated between the charges of opposite sign on the two electrodes. As a result, the thickness of the DE decreases and, due to the incompressibility of the elastomer, the membrane surface area increases at the same time. Both thickness reduction and area expansion can be used to generate actuation.

Due to their high flexibility, DEAs can be designed in many different geometries. A popular design is represented by strip-in-plane DEAs (SIP-DEAs) [31]. The basic working principle of this type of actuators is shown in Figure 1(a). SIP-DEAs can be used for applications in which a flat layout is preferred, and can also easily stacked on top of each other to increase the resulting work output [37].

In soft robotics, principles from nature are often taken as a role model. Therefore, a reasonable approach when designing DEAs for soft robotic applications would consist of using biological systems as a guide. As mentioned in the introduction, DEs are often associated to artificial muscles. The structure of human muscles, made of bundles of several fibers, serves as a design template for the RDEA used in this work. Their basic working principle is the same as for SIP-DEAs, but here the dielectric membrane and the electrodes are tightly wound in a cylindrical shape, see Figure 1 (b). In this case, the high voltage activation produces a reduction in roll diameter and, in turn, an axial expansion. RDEAs can be designed with a very slim aspect ratio (diameter < 4 mm, length > 50 mm), can be easily integrated in soft robotic structures, and can be eventually bundled together to increase the total force [34]. While working as artificial muscle-like

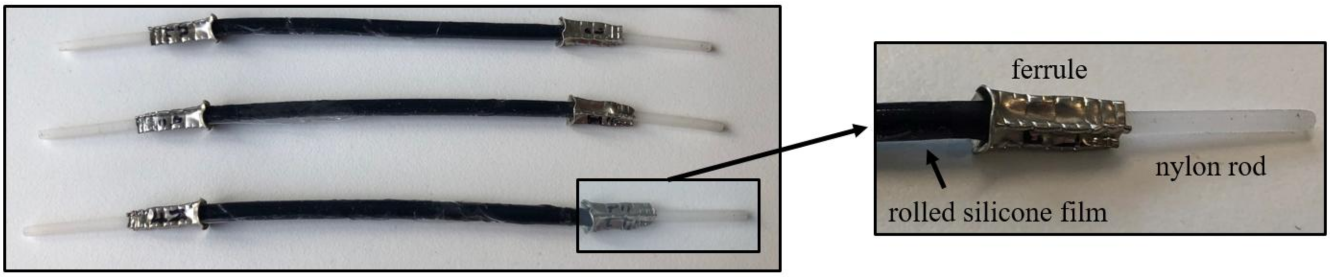

Figure 2: Picture of the manufactured RDEAs.

actuators, RDEAs can be simultaneously used as nerve-like sensor fibers. In fact, a linear relationship exists between their mechanical deformation and the resulting electrical capacitance [34]. This capacitance-based deformation estimation can be implemented during high voltage actuation, thus realizing the so-called self-sensing operating mode. This unique property is a further advantage of DEs in soft robotic applications, since one does not require additional sensors for controlling the robot in closed loop.

2.2. RDEAs design and manufacturing

The RDEAs considered in this work are manufactured based on the process presented in [34]. Rectangular electrodes (53 mm × 58 mm) with an extension for electrical contact on one side, consisting of carbon black particles suspended in a mixture of polydimethylsiloxane (PDMS), are screen printed on a 50 µm thin silicone film (Wacker Elastosil 2030). For the considered T-platform application, we restrict our investigation to this single electrode size. In this way, we were able to develop a special manufacturing rig which allows us to systematically manufacture 4 identical RDEAs at the same time. After screen printing, the films are cured in an oven. The electrodes are then tested with a voltage of 3900 V, to check for defects. If this test is passed, two electrodes with a mirrored layout are cut out and stacked on top of each other. In the subsequent step, the still planar silicone-electrodes sandwich is tightly rolled. To implement the electrical contacts, ferrules are crimped to the ends of the RDEAs and, to simplify the mounting, a nylon rod with a M2 thread is inserted at the free end of each ferrule. In order to supply a high voltage to the actuators, the RDEA ferrules need to be connected to a high voltage amplifier. This is done by screwing a cable shoe with a nut next to the ferrule on the threaded rod. A picture of the final RDEA prototype is shown in Figure 2, while its electro-mechanical characterization curves are shown in Figure 3 (obtained with the same experimental setup described in [34], in here a small viscoelastic hysteresis can be observed).

2.3. Biasing mechanism

In order to achieve a meaningful stroke, a DEA must be pre-tensioned with a suitable biasing system. In the simplest case, the biasing mechanism can be obtained via a constant load (i.e., a mass) or, more commonly, via a linear bias spring (LBS). A simple graphical method, based on a force equilibrium analysis, can be used to predict the stroke of a DEA based on the force-displacement curves of DE membrane and biasing element. An example of application of this method is shown in Figure 4(a). In here, the blue and red lines correspond to the DE characteristics for low and high voltage, respectively, while the black line corresponds to the LBS (note that, even though the LBS is a standard Hookean spring, its slope appears negative in this diagram since it is plotted with respect to the DE strain). The intersections between bias and low/high voltage DE curves represent the equilibrium positions when the actuator is turned off and on, respectively. The horizontal distance between these points coincides with the achieved stroke. Given a pair of DE curves, one can freely design the biasing element to tune the stroke accordingly, based on this simple graphical method.

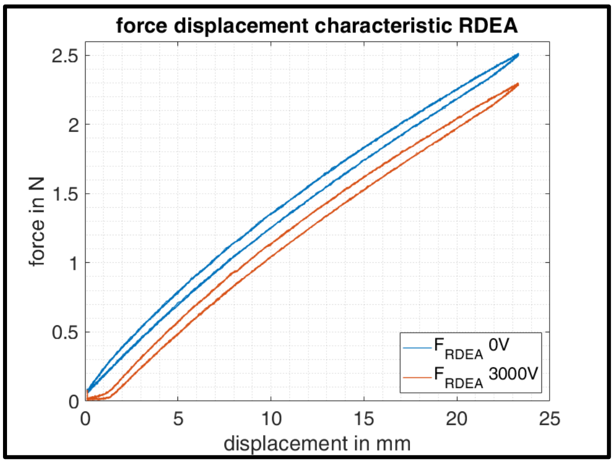

Figure 3: Force-displacement characterization curves of the manufactured RDEAs.

However, note how the use of simple elements such as masses (constant forces) or LBS results in relatively small strokes (< 10% actuation strain), compared to the deformation range achievable by the material. More complex DEA layouts make use of bi-stable biasing elements, such as pre-compressed buckled beam [31], to increase the actuation stroke. The bi-stability of such mechanisms results into a region of negative stiffness (i.e., slope) in their force-displacement characteristics, thus they are commonly referred to as negative bias

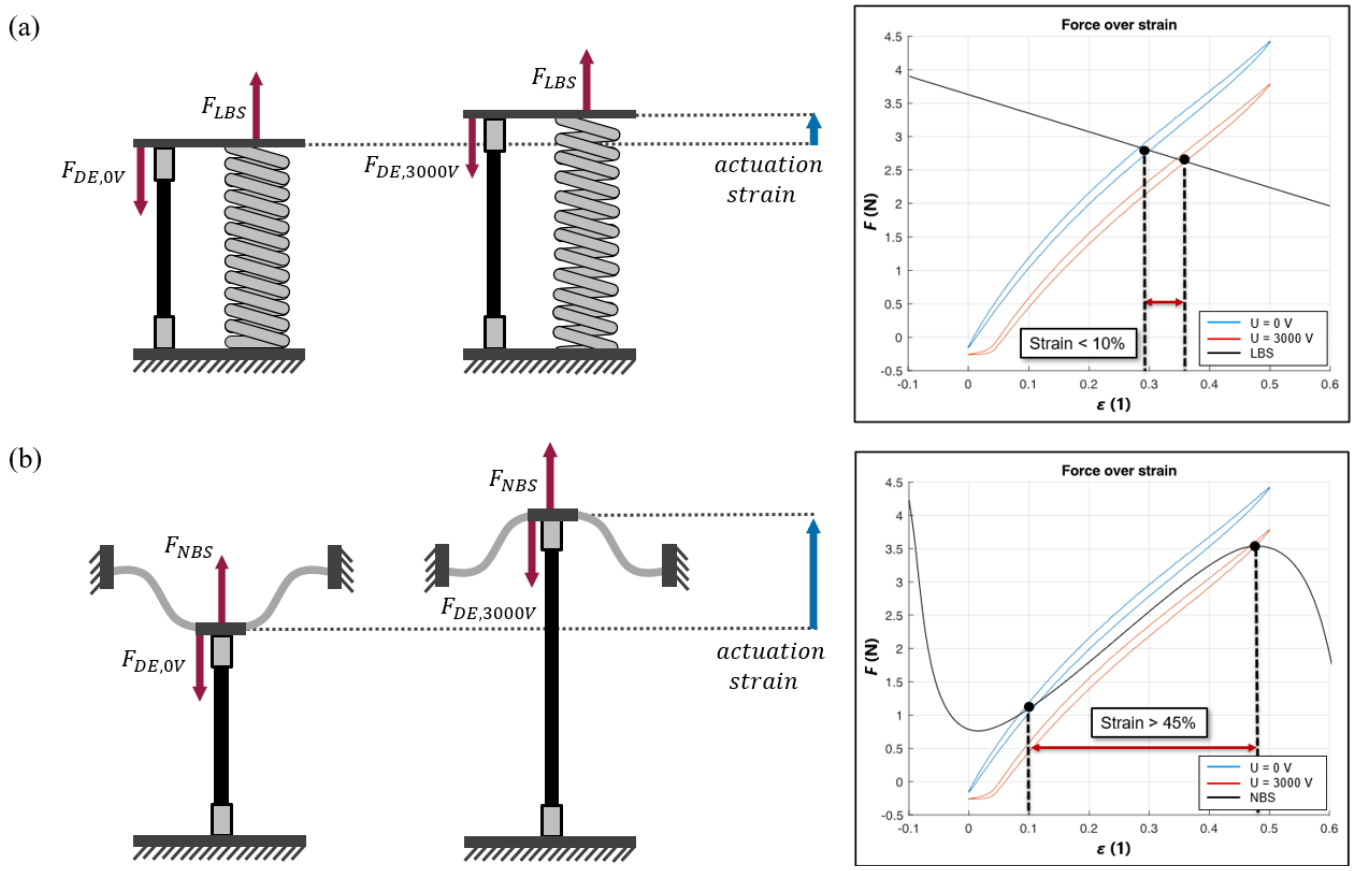

Figure 4: Force Equilibrium and graphical design of biasing mechanism: (a) LBS, (b) NBS.

spring (NBS). If this negative stiffness is properly matched with the positive stiffness of the DEA membrane, a very large stroke (> 45% actuation strain) can be achieved, as shown Figure 4(b) (also in this case, the negative stiffness of the NBS appears positive in this diagram, since its force is being plotted with respect to the DE strain). It is worthwhile mentioning how, up to date, NBS-based concepts for stroke magnification have only been applied to single-DoF DEA systems, where their design can be effectively performed graphically as described above. The desired stroke and force for the application can be set by adapting the stiffness of the LBS, or in the case of NBS the buckled beam parameters, in such a way that the force-displacement characteristic of the biasing system fits with the desired requirements into the characteristics of the DEs. For more complex DEA systems such as robots, in which several actuators are used at the same time to achieve a multi-DoF behavior, simple one-dimensional graphical methods can no longer be applied for designing the biasing elements. As a result, the high potential of DE material turns out to be highly underutilized in current DE soft robotic applications. A concept for transferring this bi-stability induced stroke magnification to multi-DoF DE systems, and demonstrating it through experiments, represents the main goal of this manuscript.

3. T-Platform Operating Principle and Parameter Study

After describing the T-platform operating principle, a discussion on the most suitable set of design parameters is presented in this section. Then, a predictive model of the T-platform is summarized and used to perform an initial performance evaluation of the system, in order to guide subsequent experimental investigations.

3.1. Operating principle

A conceptual sketch of the studied T-platform is shown in Figure 5. It consists of three main components, i.e., a flexible vertical backbone, a rigid top plate, and the RDEAs, see Figure 5(a). As for many soft robotic concepts, the nature is partly used as a role model for the T-platform operating principle. In the human upper arm, flexor and extensor work complementary as an agonist-antagonist pair [38]. In our system, the basic idea consists of using two RDEAs to replicate the role of the agonist-antagonist muscle pair. The RDEAs are mounted in a pretensioned state, with one end connected to the rigid top plate of the backbone while the other end is fixed on the base plate. Figure 5(a) shows the setup in its neutral position. Due to the pretensioning of the RDEAs, a compressive force acts

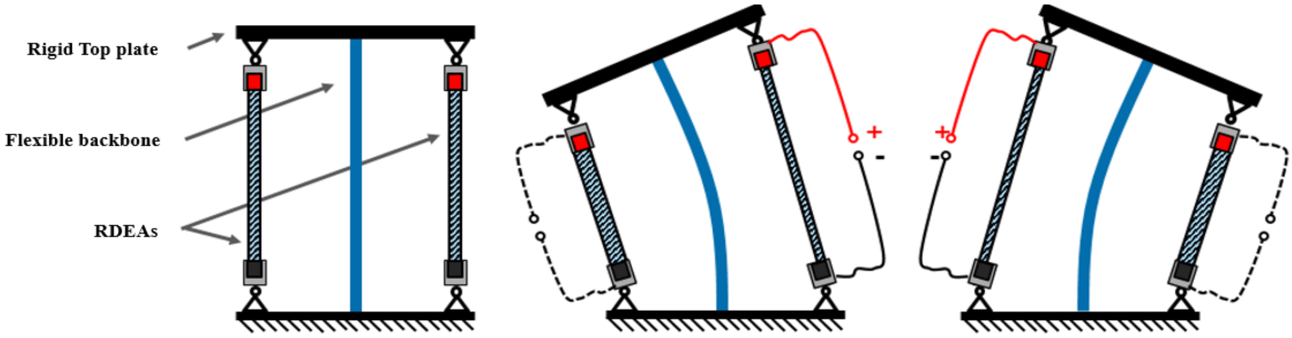

Figure 5: Operating principle of the T-platform: (a) neutral position, (b) bending when the right RDEA is actuated, (c) bending when the left RDEA is actuated.

on the top part of the flexible backbone. If a voltage is now applied to one of the actuators, the RDEAs stiffness is reduced and, as a result, the actuator force decreases accordingly. The resulting force imbalance generates a moment, which causes the backbone to bend in-plane towards the opposite direction. The motion obtained when activating the right and left RDEAs is shown in Figure 5(b) and Figure 5(c), respectively. Many of such T-platforms can be eventually stacked on top of each other, resulting into a soft tentacle arm.

One of the advantages of the proposed T-platform is represented by the possibility of exploiting the beam as a bi-stable biasing element for stroke magnification. In fact, by properly tuning the RDEAs pretensioning, the normal force acting on the beam can be made slightly larger than the buckling load. In this state, the force change due to the electrical activation of a RDEA is sufficiently large to trigger the beam buckling instability, thus causing it to snap and, in turn, produce a large bending displacement. For a detailed theoretical analysis of this phenomenon, the reader may refer to [35]. By exploiting this effect, it is possible to generalize the bi-stability induced stroke magnification concept, extensively used in case of simple DEAs [31], to the considered class of multi-DoF DE robotic structure. In this way, the actuation performance can be dramatically increased given the same amount of active material and input voltage.

3.2. Determination of the free design parameters

The T-platform is characterized by several free design parameters, which strongly affect its displacement performance. Those include the geometry of both beam and rigid plate, as well as the size and attachment points of the RDEAs. Not only those parameters are critical for determining whether the bistable actuation can be made possible, but can be also used to further fine-tune the resulting displacement range. A systematic understanding of the relationship between free parameters and resulting motion range is essential for the design of high-performance DE soft robotic systems. Since the system is characterized by a large number of design parameters, it is inconvenient to attempt optimizing all of them at the same time. In here, we will discuss a suitable subset of free design parameters for practical design optimization, whose effects on the T-platform performance will be investigated in subsequent sections.

The first and most relevant parameters are represented by the ones related to the RDEAs geometry. In fact, the shape of the RDEA force-displacement characteristics strongly depend on their geometry as well as their manufacturing process [34]. Since the relationship between RDEA geometry and their force-displacement behavior was already investigated in [34], it will not be further studied in this work. Conversely, for design convenience, we will focus on a specific actuator geometry that can be manufactured in a highly reliable way (see Section 2.2).

In addition to the RDEAs, the flexible backbone also plays a fundamental role in determining the system bending angle. The most important parameter describing the backbone flexibility, namely the bending stiffness, strongly depends on the chosen material and beam geometry [35]. A rectangular shape is considered for the cross section, to allow exploiting known results from classic beam theory for quantitative performance predictions. This results in four main free parameters for beam, namely cross-sectional thickness, cross-sectional width, length, and material (i.e., Young's modulus). Since all those parameters affect the beam bending stiffness in a lumped way, it is sufficient to change only one of them for our study. For practical design reasons, we decided to only investigate the effects of the beam thickness on the overall bending stiffness, leaving its other geometric parameters (length, width) and beam material constant.

Further free parameters result from the assembly of the various components. The attachment points of the RDEAs on the top and bottom plates strongly affect the direction along which the actuation forces are transmitted to the flexible structure, as well as the RDEA pre-stretch. Therefore, it is expected that such points have a meaningful impact on the bending performance. Since the structure needs to be symmetrical, the two attachment points on the left- and right-hand sides are selected in an equal manner. The horizontal distances from the attachment points of the RDEAs with respect to the beam top and bottom points are then chosen as further main parameters to investigate. The vertical positions of the RDEA attachment

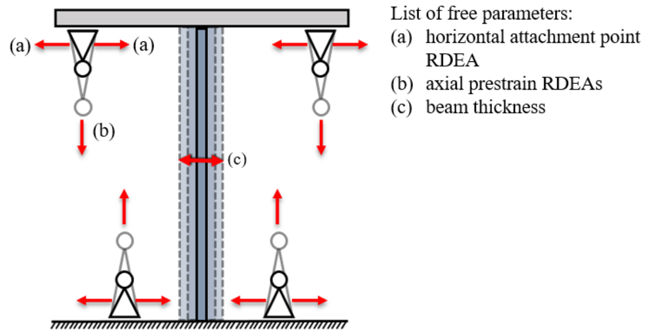

Figure 7: Free design parameters of the T-platform.

points, as well as the beam length and width, are fixed in a heuristic way compatibly with the size of the actuators discussed in Section 2.2, in order to ensure a RDEA strain of about 50% in the initial vertical position (since higher values might damage the RDEAs).

To conclude this section, we report in Figure 7 a summary of all the free quantities considered for the parameter study.

3.3. Model-based parameter study

In order to obtain a preliminary assessment of the effects of the free design parameters (i.e., upper and lower attachment points, beam thickness) on the bending performance of the T-platform, a model-based study is conducted in this section. This model allows us to establish a framework for the basic design and understanding of the bendable module and its associated theoretical performance. In this way, suitable parameter ranges can be evaluated for the subsequent experimental testing campaign.

As a first step, we summarize a physics-based, quasi-static model of the considered soft robotic system. The result is grounded on the energy-based modelling framework we previously developed for the T-platform in [35], which is here updated with our most recent version of the RDEA model [39] as well as with a novel kinematic description which accounts for the actual structure of the novel experimental setup. Figure 6(a) and Figure 6(b) depict a schematic representation, the T-platform in both undeformed and deformed configurations, respectively. In here, all the relevant system component and geometric parameters are also highlighted. The model essentially comprises three main elements of the T-platform, namely the rigid top plate, the flexible beam, and the RDEAs. For simplicity, we assume that the geometric state of the beam and RDEAs is uniquely determined once the configuration of the top plate is fixed (see [35] for details). For a planar motion, this allows us to completely describe the system with the following vector of generalized coordinates

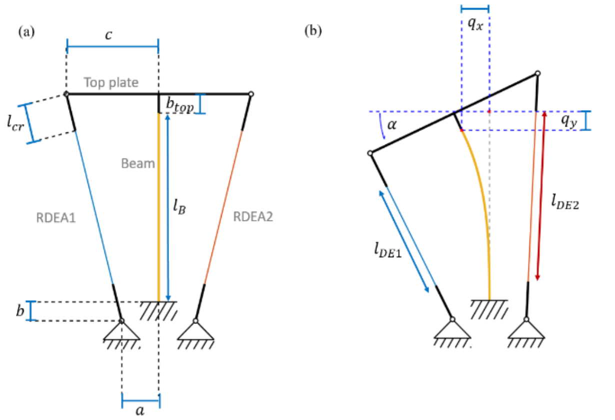

Figure 6: Sketch of the T-platform kinematic model, (a) undeformed configuration, (b) deformed configuration.

$$q = \begin{bmatrix} q_x \\ q_y \\ \alpha \end{bmatrix}, \tag{1}$$

whose components correspond to the horizontal and vertical displacement of the beam tip, as well as the orientation of the top plate, respectively (cf. Figure 6(b)). According to Lagrangian mechanics, the system equilibrium configurations are given by the solutions of the following system of equations

$$\frac{\partial \mathrm{V}}{\partial q} = 0, \tag{2}$$

where ς is the total potential energy of the system. In our case, ς can be expressed as the sum of three sub-components, i.e.,

$$\mathrm{V} = \mathrm{V}_{TP} + \mathrm{V}_B + \mathrm{V}_{DE}, \tag{3}$$

representing the gravitational potential energy of the top plate, the elastic potential energy of the beam, and the electro-mechanical potential co-energy of the RDEAs, respectively. ς_{TP} and ς_B can be expressed as a function of q as follows [35]

$$\mathrm{V}_{TP}(q) = m_{TP} g \left(l_B + q_y + b_{top} \cos \alpha \right), \tag{4}$$

$$\mathrm{V}_B(q) = \frac{E_B I_B}{2 l_B} \left[q^T S^T G S q + \frac{\left(\frac{q_y}{l_B} + \frac{1}{2} q^T S^T P S q \right)^2}{\frac{I_B}{A_B l_B^2} - q^T S^T Q S q} \right], \tag{5}$$

where

$$S = \begin{bmatrix} l_B^{-1} & 0 & 0 \\ 0 & 0 & 1 \end{bmatrix}, \quad G = \begin{bmatrix} 12 & -6 \\ -6 & 4 \end{bmatrix},$$

$$P = \begin{bmatrix} \frac{6}{5} & -\frac{1}{10} \\ -\frac{1}{10} & \frac{2}{15} \end{bmatrix}, \quad Q = \begin{bmatrix} -\frac{1}{700} & \frac{1}{1400} \\ \frac{1}{1400} & -\frac{11}{6300} \end{bmatrix},$$

m_{TP} is the rigid top platform mass, g is the gravitational constant, l_B is the undeformed beam length, E_B is the Young's modulus of the beam material, I_B is the beam second moment of area, and A_B is the beam cross-sectional area. By assuming a beam with a rectangular cross-section with width w_B and thickness t_B, we can simply compute the last two beam parameters as $I_B = w_B t_B^3/12$ and $A_B = w_B t_B$. In order to define the DE electro-mechanical energy, we first need to define two additional quantities, i.e., the vector of DE voltages v_{DE}

$$v_{DE} = \begin{bmatrix} v_{DE1} \\ v_{DE2} \end{bmatrix} \tag{6}$$

as well as the vector of DE lengths l_{DE} (cf. Figure 6(b))

$$l_{DE}(q) = \begin{bmatrix} l_{DE1}(q) \\ l_{DE2}(q) \end{bmatrix},$$

$$l_{DE1}(q) = \left\| \begin{bmatrix} q_x - b_{top}\sin\alpha - c\cos\alpha + a \\ l_B + q_y + b_{top}\cos\alpha - c\sin\alpha - b \end{bmatrix} \right\| - 2l_{cr}, \tag{7}$$

$$l_{DE2}(q) = \left\| \begin{bmatrix} q_x - b_{top}\sin\alpha + c\cos\alpha - a \\ l_B + q_y + b_{top}\cos\alpha + c\sin\alpha - b \end{bmatrix} \right\| - 2l_{cr},$$

where subscript i refers to RDEA i, i = 1, 2, l_{cr} takes into account the length of the passive crimps connecting the RDEAs to the T-platform pivot points, and all the other geometric parameters are reported in Figure 6. Then, based on (6), (7), the total co-energy of the RDEAs can be expressed as follows [35], [39]

$$\mathrm{V}_{DE}\left(l_{DE}(q), v_{DE}\right) = \sum_{i=1}^{2} \left[\sum_{j=1}^{3} 2L_1L_2L_3C_{j0} \left(\frac{l_{DEi}^2(q)}{L_1^2} + 2\frac{L_1}{l_{DEi}(q)} - 3 \right)^j - \frac{\alpha_{e1}\eta_b \epsilon_0 \epsilon_r L_2 l_{DEi}(q)}{L_3} v_{DEi}^2 \right], \tag{8}$$

where L_1, L_2, L_3 are the RDEAs principal lengths in undeformed configuration, C_{j0} are Yeoh parameters describing the DE material hyperelastic response, j = 1, 2, 3, α_{el} an η_b are volumetric loss factors of the RDEA, ϵ_0 is the vacuum permittivity, and ϵ_r is the DE relative permittivity. The complete set of equations describing the T-platform steady-state response can be obtained by replacing (4), (5), (7), (8) in (3) (explicit computations are straightforward but cumbersome, thus they are omitted here for conciseness). In this way, we can compute the system equilibrium configurations resulting from the application of a given pair of input DE voltages.

The developed model is then used to perform some initial parameter studies, aimed at understanding the trends of how the bending angle α varies as a function of the free design parameters shown in Figure 7, i.e., upper RDEA attachment point c, lower RDEA attachment point a, beam thickness t_B. All the other model parameters are assumed to be known in advance. In particular, the beam length and width, as well as the constant geometric parameters of the structure, are fixed in a heuristic according to the guidelines provided at the end of Section 3.2. The DE material parameters are obtained based on the RDEA characterization in Figure 3, while the beam Young's modulus and the top-plate mass are determined based on known properties of available 3D printing materials (i.e., PETG [40], Rigid 10K Resin [41], see Section 4 for more details). The numerical values used for all the constant parameters are summarized Appendix. Simulations are then conducted by choosing different values of a, c, t_B, and, and the resulting performance of the T-platform is examined. In each case, only one RDEA is activated with a voltage of 3000 V, while the other one is kept at 0 V. For each combination of parameters, Figure 8 shows the maximum deflection angle α and the corresponding maximal RDEA strain (whose computation is based on the roll axial stretch, according to [39]). From the results in Figure 8, it can be seen that α increases for smaller distances between the actuators and the beam, independently of whether it is the top distance c or the bottom one a, and the same holds true for decreasing beam thickness t_B. The maximum bending performance, indeed, is obtained for c = 18 mm, a = 15 mm, and t_B = 1.35 mm, and is predicted to be of about 24°. Following the approach in [35], we analyzed the stability of the T-platform for this set of parameters, in both unactuated and actuated states. It is revealed that, for this specific combination of parameters, the unactuated T-platform is indeed bistable, while it is monostable when in its actuated configuration at 24°. The trends in Figure 8 are consistent with the physics of the problem. In fact, thinner beams tend to buckle at lower compressive forces, and thus the resulting bending angle increases given the same RDEAs pre-tension. If the beam thickness is reduced too much, however, the normal stress becomes so large that activating the RDEA no longer causes a buckling to the opposite direction. In this case, not only the unactivated T-platform, but also the actuated one, turns out to be bi-stable. As a result, reversibility of the actuation is lost, and the design becomes no longer effective. Placing the actuators closer to the backbone, instead, increases the bending angle because the same change in RDEA length results in a larger beam displacement, due to the stronger kinematic coupling among the two. The corresponding maximal RDEA strain diagrams, depicted in the lower part of Figure 8, show that the parameter combination corresponding to maximum bending angle is close to 50%, which represents the maximum allowed strain for the considered rolls. Smaller beam-RDEA distances or beam thickness values would result in higher maximal strains, which would then exceed our safety limit value. Conversely, configurations with bigger beam-RDEA distances of beam thickness would result into mono-stable configurations which lead to a poor bending angle performance, and thus they are not relevant in practical applications. By using the model, one can find the parameters which maximize the bending performance while resulting into a functional T-platform design, i.e., the actuated configuration always exhibits only one stable equilibrium and the RDEAs must not be overstretched. Based on the above considerations and practical design trade-offs, we choose the following parameter ranges for the subsequent experimental investigation:

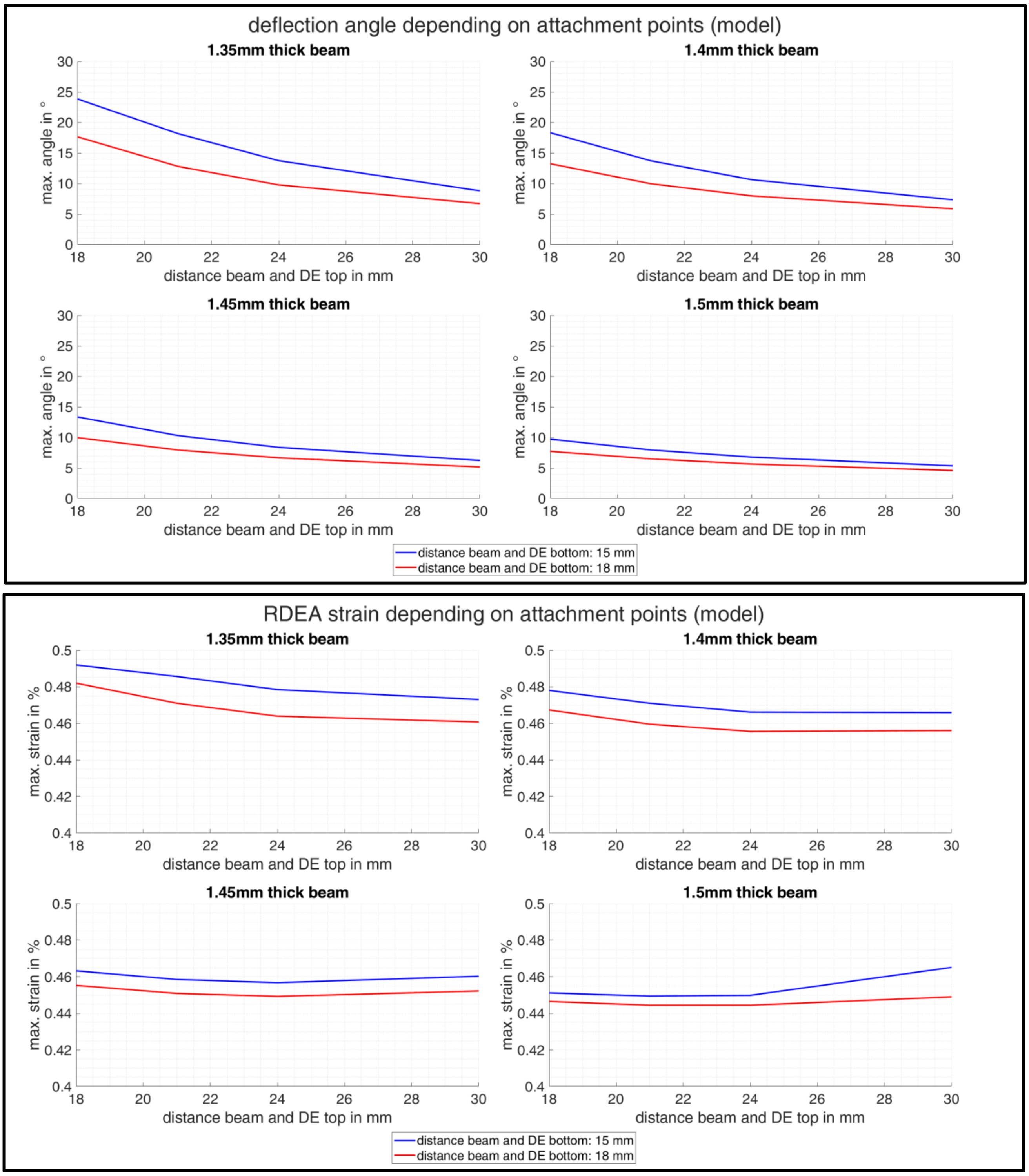

Figure 8: Model-based parameter study, T-platform bending angle (upper part) and maximum RDEA strain (lower part).

distance between RDEA upper part and beam $c \in [18, 30]$ mm; distance between RDEA lower part and beam $a \in [15, 18]$ mm; beam thickness $t_B \in [1.35, 1.5]$ mm.

As a final remark, we include some considerations on the maximum electric field, which is related to electrical breakdown in the DE. The electric field of RDEA i, $i = 1, 2$, is given by [39]

$$E_i = \sqrt{\frac{l_{DEi}(q)}{L_1}\frac{v_{DEi}}{L_3}}, \quad i = 1,2. \tag{9}$$

For the maximum DE length obtained in simulation, a peak electric field of about 73.5 V/μm is computed. Since this is always smaller than the safety value of 80 V/μm recommended by the elastomer manufacturer, we can consider the system suitable from an electrical viewpoint.

4. T-Platform Manufacturing and Assembly

In order to experimentally validate the performance predicted by the model-based study, the overall T-platform design must guarantee the possibility of varying the parameters of interest independently of each other, within their ideal range of variation determined in Section 3.3. A suitable physical realization for such a design is discussed in this section.

To ensure consistency with the theoretical T-platform concept in Figure 5, the connection between actuators and platform should allow the RDEAs to spontaneously orient itself along the line passing through the top and bottom attachment points. Furthermore, the horizontal distance between the center of the platform and the attachment points should be freely variable, and the vertical position of the attachment point should be precisely adjustable as well. The free alignment is ensured by an adapter mounted on the threaded rod of the RDEAs, which has a triangular profile on both sides. This profile is hooked into a larger triangular notch in the rigid platform, as shown in Figure 9. The adapter is held in place by the tensile force of the RDEA, which presses it against a nut serving as a mechanical stop. Due to the size difference between the triangular notch and the adapter, the profile can rotate freely in the notch, and thus it can always adjust its direction according to the one of the RDEA force. The horizontal distance to the platform center can be varied by placing several notches at different distances from the central axis of the beam, see Figure 9. The nut, which serves as stop for the attachment adapter, can be used at the same time to finely adjust the vertical position. Six notches are provided on the top plate, equally spaced with an offset of 3 mm. Therefore, the attachment point of the RDEAs can be varied from 18 mm to 30 mm with steps of 3 mm. Two notches are provided onto the lower platform, placed at a distance of 15 mm and 18 mm, respectively.

For connecting the flexible beam to the base and top plates, a screw-based clamping device is incorporated into the design of both plates. The beam is simply inserted into a gap on the two plates, so that it can be manually replaced in a simple way. To allow accurate insertion of beams with different thickness at the center of the gap, 3D printed rubber plates are used as adapters. In the last step, the beam is fixed with two screws on each side.

Figure 10(a) shows the CAD model of the final T-platform. The rigid top plate and the bottom plate are printed with a SLA 3D printer. The SLA printer ensures an accurate resolution of the notches. Due to their fine profile structure, the adapters for RDEA attachment are also fabricated with the same printer. A

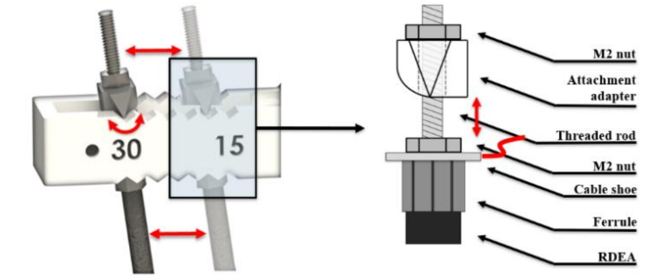

Figure 9: Structure for RDEA attachment and tuneable mounting point on the T-platform.

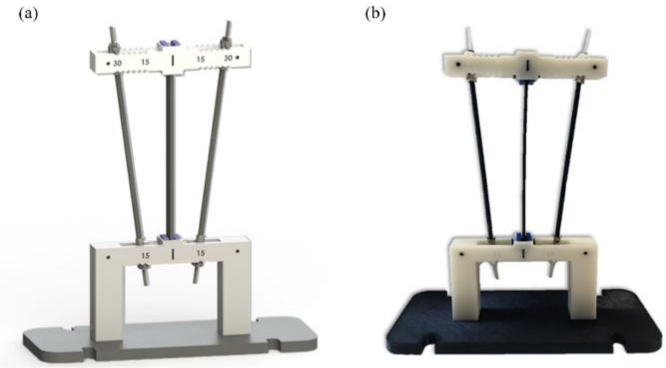

Figure 10: Assembled T-platform: (a) CAD Model, (b) first experimental prototype.

bottom plate filament, printed out of PETG, is used to rigidly connect the T-platform to the test bench. Once in this configuration, the RDEAs and the backbone can be mounted between the two plates. For the backbone fabrication, a selection of different PETG beams are printed with the filament printer, according to the geometry provided in the Appendix (i.e., length of 110 mm, width of 10 mm, thickness ranging between 1.35 mm and 1.5 mm). PETG is chosen as beam material, due to its smaller viscoelastic creep and higher repeatability in comparison to other available 3D printed materials (e.g., TPU). A picture of the resulting first prototype is shown in Figure 10(b).

5. Experimental Results

This section presents an experimental characterization of the T-platform, together with an experimental validation of the parameter study.

5.1. Experimental test rig

A custom test rig is assembled to systematically characterize the T-platform, and evaluate the performance achieved with different design parameters. For each combination of pa-

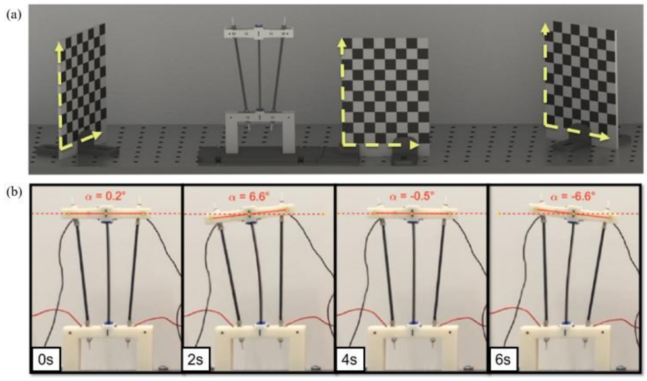

Figure 11: Experimental setup for characterization of the T-platform: (a) test rig with reference coordinate systems, (b) deflection angle tracking in video.

rameters, an experiment is conducted in which different periodic voltage signals are alternately applied to the left and right RDEA. Two high voltage amplifiers available in our lab (Hivolt HA51U, Ultravolt 4HVA) are used for this purpose, both of them compatible with the voltage/capacitance range of the RDEAs. During this process, a camera is used to record the motion of the module. The test rig allows to automatically detect the position of the T-platform, track its motion over time, and compute the resulting bending angle.

To make the setup as independent as possible from focus settings and camera position, those parameters should be automatically recognizable by (and account for) the motion tracking algorithm. To this end, the MATLAB “Camera Calibrator” app is used to extract those parameters through at least two reference coordinate systems located in different planes. In order to recognize the coordinate systems during the video post-processing, three tilted plates with a chessboard pattern are placed in the test rig. Note that two of the chessboard plates are out of plane with the T-platform and one plate in plane with the T-platform. By means of an image recognition algorithm, it is possible to identify the individual corners of the chessboard, and use them to generate a coherent coordinate system. The two out of plane coordinate systems are used in the calibration app to get the camera settings. And the third one as reference coordinate system for the T-platform. The complete arrangement of T-platform and three chessboard plates is portrayed in Figure 11(a).

To further assist the motion tracking algorithm, three markers are placed on both the base and the top plate of the T-platform (i.e., two black dots and a vertical line for each element), also visible in Figure 10. The marked positions on the T-platform can now be determined with respect to the reference coordinate systems. Once the positions of all the T-platform relevant points are obtained, their motion can be tracked in the video. In the last step, the bending angle can be computed from the positions of the moving points by using standard rigid body kinematics. The result of this tracking algorithm for the angle of deflection is shown in Figure 11(b).

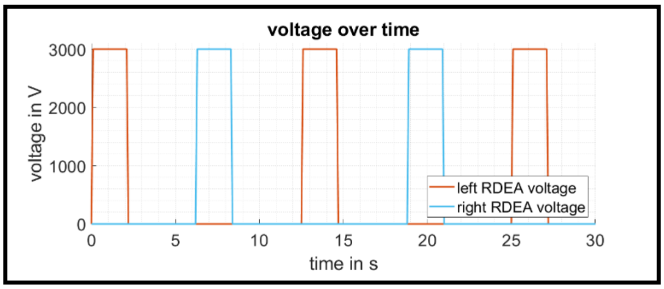

Figure 12: Applied voltage signal to the actuators for experimental investigation.

5.2. T-platform actuation performance and parameter study

The developed test rig can be used to determine the relationship between the bending angle and the various parameters discussed in Section 3. Other than just analyzing the angular displacement performance, it is also meaningful to investigate for which combinations of parameters the system is bi-stable, and how the bi-stability feature affects the maximum deflection angle. The performance of different prototypes are measured, by considering all the possible combinations of the following parameters (for a total of 32 experiments):

- Top DE distance c: 18 mm, 21, mm, 24 mm, 30 mm;
- Bottom DE distance a: 15 mm, 18 mm;
- Beam thickness t_B: 1.35 mm, 1.4 mm, 1.45 mm, 1.5 mm.

Note that the configurations corresponding to c = 27 mm are omitted, since they led to almost identical performance compared to the 30 mm case.

During the measurements, a square wave voltage signal with a duration of 2 s and a constant amplitude of 3000 V is applied alternately to the two actuators, in such a way that both rolls remain inactive for 4 s between activations. An example of such a signal is shown in Figure 12.

In the first step of the experimental campaign, the bending angle is determined over time according to the procedure described in Section 5.1. Based on the time behavior of the angle, statements can already be made concerning the bi-stability of the system. To better clarify the meaning of bi-stability in the context of our system, Figure 13 shows an example of time behavior of the T-platform bending angle, for both a mono-stable (a) and a bi-stable (b) configuration. The mono-stable case corresponds to c = 30 mm, a = 18 mm, and t_B = 1.4 mm. With this combination of parameters, the T-platform reaches a maximum deflection around 6°, and the system returns to the neutral position when the voltage is switched off. In contrast, an example of bi-stable case corresponds to c = 18 mm, a = 15 mm, and t_B = 1.35 mm. With this combination of parameters,

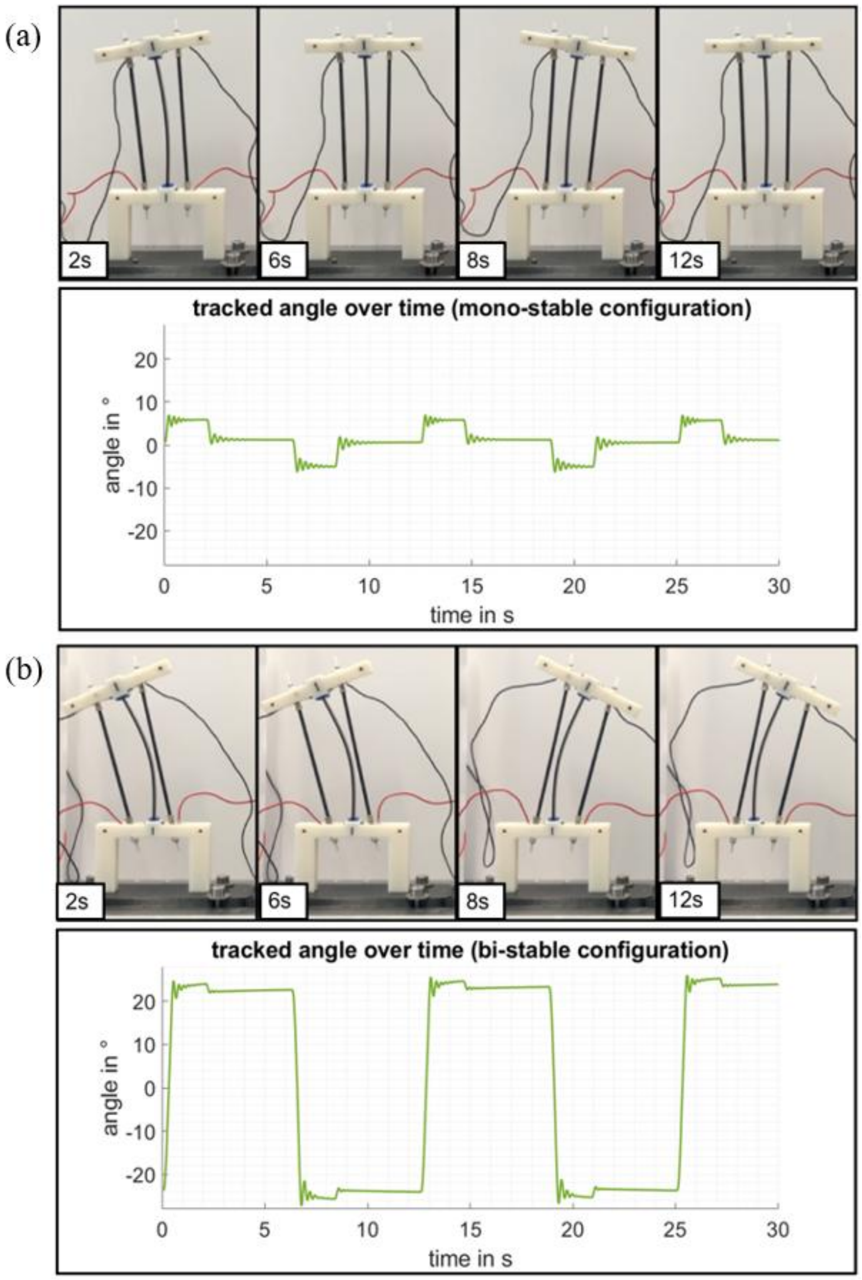

Figure 13: Experimental investigation of the T-platform, (a) mono-stable system corresponding to c = 30 mm, a = 18 mm, and t_B = 1.4 mm, (b) bi-stable system, corresponding to c = 18 mm, a = 15 mm, and t_B = 1.35 mm.

the T-platform reaches a maximum deflection around 25°. After the voltage is switched off, the system does not come back to the neutral position (as for the mono-stable case), but rather settles to a deflection angle of about 22°. This behavior can be observed with respect to the actuation along both directions. The system therefore snaps from one stable equilibrium position to a second one when the voltage is applied, and is therefore bi-stable. Other than proving a larger bending angle, the bi-stable actuation also provides energy saving features, since it allows to maintain a non-zero bending angle without the need of supplying any electrical power. This might represent a further advantage in energy-critical applications, e.g., mobile ones.

After clarifying the role of bi-stability in determining the T-platform time behavior, we discuss the results of the experimental study. Figure 14 shows the relationships between the attachment points and the resulting maximum bending angle, for all the considered combinations of parameter. Each experiment is represented with a circle, which are superimposed to continuous lines that represent the simulation results from Section 3.3. As expected from the theoretical investigation, we can achieve a wide spectrum of possible bending angles,

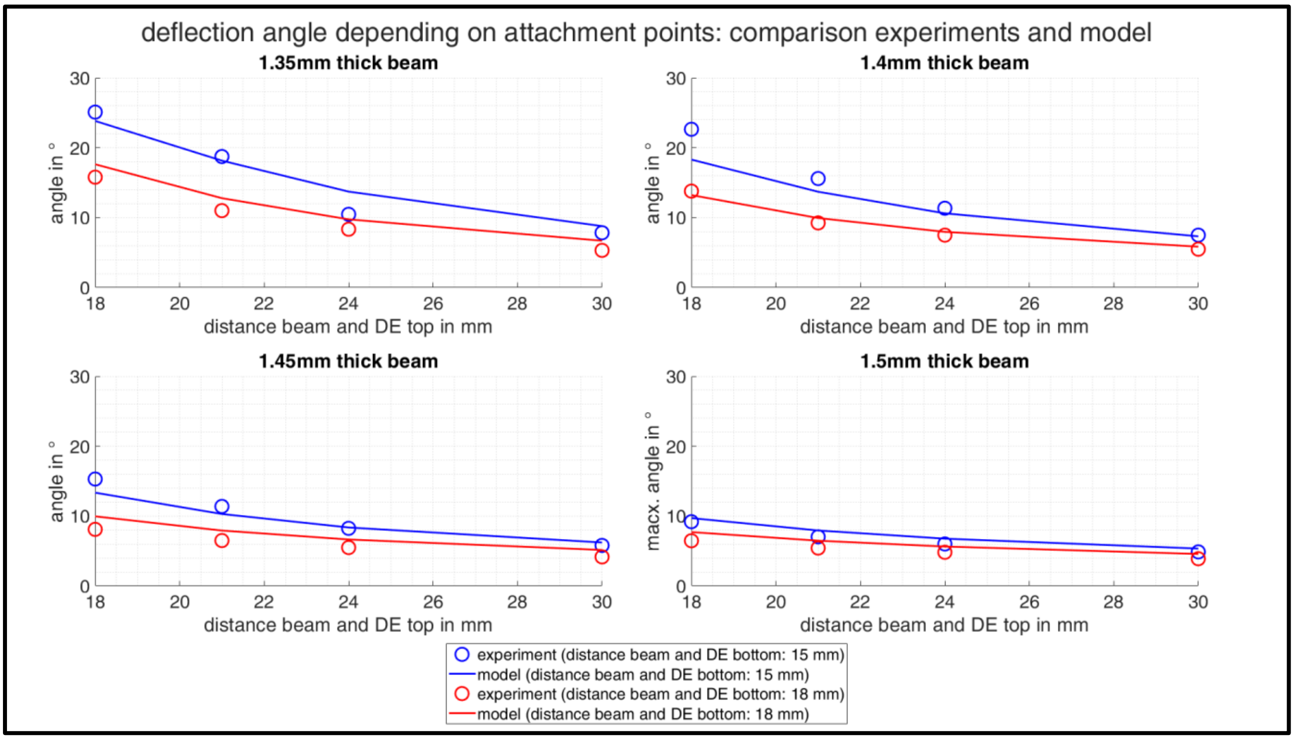

Figure 14: Experimental investigation of the deflection angle depending on the attachment points for different beams, and comparison with model data.

which range from 5° up to 25°. The experimental results also show a remarkable agreement with the simulated curves. Some deviations exist, mostly visible for the $t_B = 1.4$ mm case, which are reasonably due to manufacturing tolerances as well as due to the introduction of simplifying assumptions in the derivation of the beam model. Nevertheless, the trends are reproduced in a remarkable way, and the maximum bending angle of 25° was predicted by the model with an error of 1°. The obtained results confirm then the effectiveness of our bi-stable design principle, and confirm that our model represents a valuable numerical tool to systematically optimize the T-platform design.

By inspecting the results, it is observed that bending angles larger than a given threshold value always correspond to a bi-stable behavior, independently of the choice of the beam and other parameters. Such a threshold is small for thinner beams, and becomes higher for thicker beams. As an example, in the case of the thinnest beam ($t_B = 1.35$ mm), the system is always bi-stable for bending angles when the bending angle is larger than 7.8°. With thicker beams, the system only becomes bi-stable at larger angles of deflection (11.2° for a 1.45 mm thick beam). Figure 15 summarizes the experimental results from Figure 14 in two plots, and groups together the different configurations which result in a mono-stable (blue region) and bi-stable (red region) behaviors. From this plot, it is evident how the bi-stable configurations generally lead to much higher bending angles than mono-stable designs. This confirms that bi-stable biasing mechanisms permit to increase the actuation

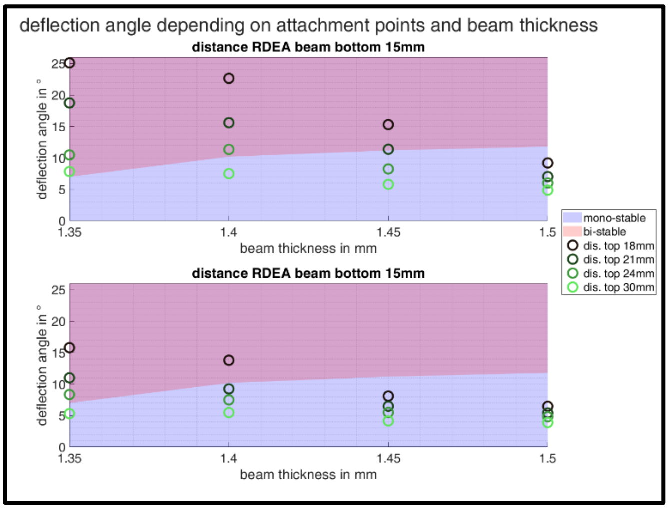

Figure 15: Parameter study on the T-platform: correlation deflection angle and beam thickness.

displacement not only for single-DoF DEAs, but also to multi-DoF DE soft robotic structures. Such a result represents then the first successful experimental verification of the bi-stable actuation concept initially theorized in [35].

In conclusion, we have verified experimentally that, in order to maximize the actuation performance, one should move the RDEAs as close as possible to the beam and select a sufficiently thin beam. This combination of parameters will favor buckling which, in turn, leads to a large bending performance.

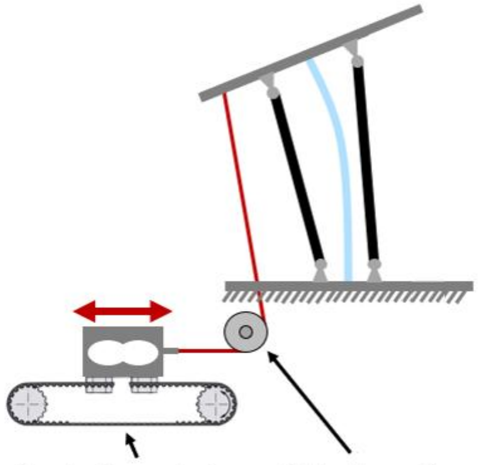

Figure 16: Experimental setup to measure the mechanical compliance.

The buckling, however, should not be favored too much, otherwise the actuation becomes irreversible, causing the system no longer to snap when the opposite RDEA is activated. The optimal trade-off between large bending angle and reversible actuation can be tuned via an appropriate choice of the free parameters, and can be eventually supported by the proposed physics-based model. Those finding will provide useful guidelines for the design of future soft tentacle arms based on stacks of many T-platforms.

5.3. Suitability for soft robotics applications

To conclude this section, we investigate the suitability of the T-platform for soft robotic applications. To this end, we perform experiments aimed at evaluating the prototype compliance when subject to an external deformation, since this property is important to ensure a safe human-robot interaction. To measure the T-platform compliance, the setup shown in Figure 16 is used. A steel rope (depicted in red) is wired parallel to the left RDEAs, the rope is connected to a load cell (ME-Meßsysteme KD40s) via pulleys. This load cell is mounted on a linear drive, whose displacement can be arbitrarily prescribed.

In order to measure parameters related to the structure mechanical compliance, tensile experiments are carried out for both mono- and bi-stable configurations (mono-stable: c = 18 mm, a = 18 mm, t_B = 1.4 mm; bi-stable: c = 24 mm, a = 18 mm, t_B = 1.4 mm). By prescribing a deformation profile to the linear actuator, the structure bends accordingly. During this process, we acquire the force of the load cells, as well as the angle of the rigid spacer mounted at the top of the flexible beam. In order to extract a meaningful compliance measure from those data, we use standard rigid body dynamics to convert the forces to the equivalent moment applied to the center of mass of the rigid spacer. In this way, we can plot the moment as a function of the bending angle, and extract the angular compliance by measuring the slope of this diagram. The corresponding plots are shown in Figure 17.

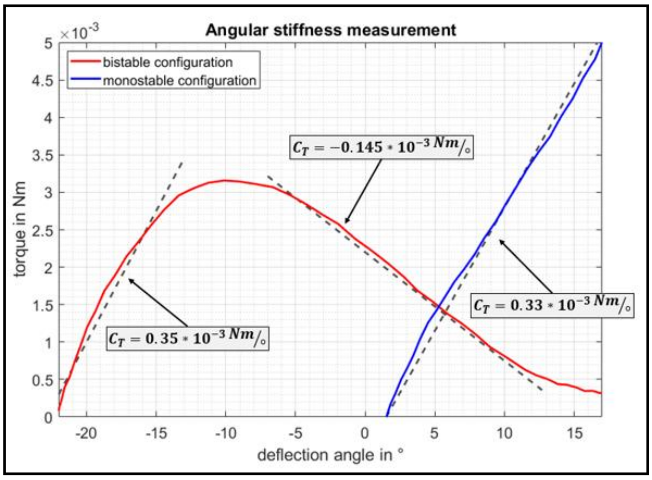

Figure 17: T-platform angular stiffness measurement.

For the monostable case, there is a linear relationship between the deflection angle and the torque. The corresponding angular stiffness is C_T = 0.33·10^{-3} Nm/°. In contrast, the bistable design results in a non-linear relationship with a region of positive stiffness (C_T = 0.35·10^{-3} Nm/°) and a region of negative stiffness (C_T = -0.15·10^{-3} Nm/°). This behaviour is equivalent to that of a mono- and bi-stable biasing mechanism with an LBS or NBS in single-DoF. For comparison, the angular stiffness of the human muscle in the elbow is in a range of C_{Tmin} = -0.35 Nm/° up to C_{Tmax} = 0.35 Nm/° [42]. Therefore, our T-platform is softer by a factor of 10^3 compared to human muscles, thus confirming its suitability for soft robotics and safe human-robot collaboration.

6. Conclusion

In this work, the first concept of a bendable soft robotic module, consisting of a pair of silicone-based RDEAs actuating a flexible T-platform, was presented and experimentally validated for the first time. The influence of the free design parameters (i.e., beam thickness, RDEA upper and lower mounting points) on the bending angle performance was systematically investigated by means of both simulation studies and experimental investigations. It was found that the bending angle strongly depends on such parameters, and can range between 5° and 25° for the considered parameter space, given the same RDEA geometry and actuation voltage. A good adherence is also observed between simulations and experiments, thus confirming the proposed model as a valuable tool to optimize the T-platform performance. It was also found that, for some combinations of parameters, the system exhibits

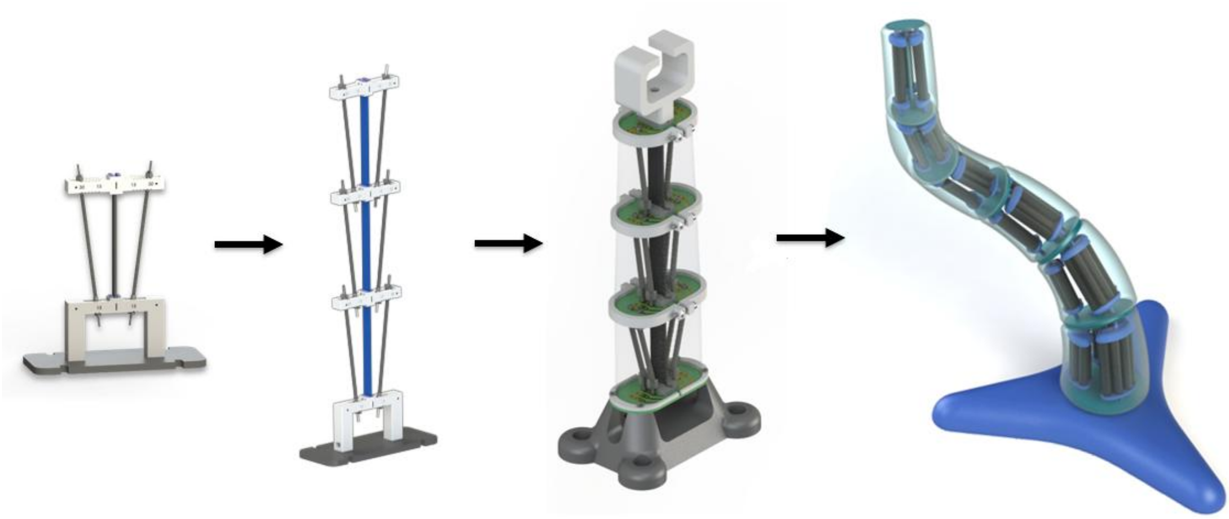

Figure 18: Future planned development steps in the way to a DE-based soft robot arm

a controllable bi-stable behavior which, in turn, results in much larger bending angles compared to mono-stable configurations. These findings confirm that, similar to what happens to single-DoF DEAs, bi-stable biasing concepts can be also successfully used to increase the performance of multi-DoF DE structures. The bi-stability also makes it possible to keep the robot in a deformed state without spending electric energy, while mono-stable configurations require a continuous supply of electric power to maintain a desired deflection. These findings confirm that, similarly to what happens to single-DoF DEAs, bi-stable biasing concepts can be also successfully used to increase the performance of multi-DoF DE structures. For the best possible combination of parameters, the maximum deflection angle could be increased up to 25°. Such a value is more than 2.5 larger than our previous concept for silicone-based DE rotational module, which could only bend up to 9.6° for the best possible combination of design parameters [30]. Finally, angular compliance measurements confirmed that our T-platform is softer than human muscles by a factor of 10^3, thus confirming its suitability for soft robotic applications.

The promising performance of the considered T-platform opens up several possible future directions for our research. Full DE soft tentacle arms will be developed based on stacks of several T-platforms, as shown in Figure 18. Stacking several modules presents new challenges for the design. In this case, in fact, the influence of the weight and moment of the upper platforms must be balanced out by the lower platforms, and electrical contacts to the upper modules must also be ensured. Thus, in the future, scaling the force by bundling RDEAs, and finding new ways to contact them electrically, will also be important points to investigate. Scaling the force will also allow the robot arm to adapt to real applications, which involve manipulation of objects. Regarding this aspect, external load forces and moments are also expected to impact the system bi-stability, so that their effects will be explicitly investigated (and accounted for) in future designs. The bi-stable design will also be extended beyond the planar actuation, in order to enable bending along all spatial directions. At the same time, the model will be also validated in a dynamic setting, and will be used to develop motion/interaction control strategies as well as self-sensing estimation of the robot configuration. In this way, we will be able to achieve proportional stabilization of intermediate angles, and thus achieve proportional control of the bending angle while keeping the large displacement benefits of the bi-stable design.

Appendix: parameters used in the simulation study

Top plate parameters: m_{TP} = 12 g, g = 9.81 m/s^2.
Structure parameters: b = 15 mm, b_{top} = 15 mm, l_{cr} = 13.8 mm.
Beam parameters: l_B = 110 mm, w_B = 10 mm, E_B = 1.9 GPa.
RDEA parameters: L_1 = 68.2 mm, L_2 = 78 mm, L_3 = 47.6 µm, C_{10} = 218000 Pa, C_{20} = -24000 Pa, C_{30} = 16000 Pa, α_{e1} = 0.74, η_b = 0.74, ϵ_r = 2.8, ϵ_0 = 8.85·10^{-12} F/m.

Acknowledgements

The authors gratefully acknowledge the support of the Deutsche Forschungsgemeinschaft (DFG, German Research Foundation) through Priority Program SPP 2100 "Soft Material Robotic Systems" (Projects: SE704/6-1, RI3030/1- 1).

References

[1] M. Vasić and A. Billard, "Safety issues in human-robot interactions," *2013 IEEE International Conference on Robotics and Automation*, pp. 197–204, 2013.

[2] K. M'Colo, B. Luong, A. Crosnier, C. Neel, and P. Fraisse, "Obstacle Avoidance using a Capacitive Skin for Safe Human-Robot Interaction.," Oct. 2019, pp. 6742–6747. doi: 10.1109/IROS40897.2019.8967605.

[3] A. Vysocky and P. Novak, "Human - Robot collaboration in industry," *MM Science Journal*, vol. 2016, pp. 903–906, Oct. 2016, doi: 10.17973/MMSJ.2016_06_201611.

[4] G. Runge *et al.*, "SpineMan: Design of a soft robotic spine-like manipulator for safe human-robot interaction," in *2015 IEEE/RSJ International Conference on Intelligent Robots and Systems (IROS)*, 2015, pp. 1103–1110. doi: 10.1109/IROS.2015.7353508.

[5] D. Rus and M. T. Tolley, "Design, fabrication and control of soft robots," *Nature*, vol. 521, no. 7553, pp. 467–475, 2015, doi: 10.1038/nature14543.

[6] X. Zhou, Y. Teng, and X. Li, "Development of a new pneumatic-driven earthworm-like soft robot," in *2016 23rd International Conference on Mechatronics and Machine Vision in Practice (M2VIP)*, 2016, pp. 1–5. doi: 10.1109/M2VIP.2016.7827269.

[7] G. Borghesan, G. Palli, and C. Melchiorri, *Design of tendon-driven robotic fingers: Modeling and control issues*. 2010. doi: 10.1109/ROBOT.2010.5509899.

[8] N. Kastor, R. Mukherjee, E. Cohen, V. Vikas, B. A. Trimmer, and R. D. White, "Design and Manufacturing of Tendon-Driven Soft Foam Robots," *Robotica*, vol. 38, no. 1, pp. 88–105, Jan. 2020, doi: 10.1017/S0263574719000481.

[9] P. Boyraz, G. Runge, and A. Raatz, "An Overview of Novel Actuators for Soft Robotics," *Actuators*, vol. 7, no. 3, 2018, doi: 10.3390/act7030048.

[10] U. Gupta, L. Qin, Y. Wang, H. Godaba, and J. Zhu, "Soft robots based on dielectric elastomer actuators: a review," *Smart Mater Struct*, vol. 28, no. 10, p. 103002, Sep. 2019, doi: 10.1088/1361-665x/ab3a77.

[11] I. A. Anderson, T. A. Gisby, T. G. McKay, B. M. O'Brien, and E. P. Calius, "Multi-functional dielectric elastomer artificial muscles for soft and smart machines," *J Appl Phys*, vol. 112, no. 4, p. 41101, 2012, doi: 10.1063/1.4740023.

[12] Y. Qiu, E. Zhang, R. Plamthottam, and Q. Pei, "Dielectric Elastomer Artificial Muscle: Materials Innovations and Device Explorations," *Acc Chem Res*, vol. 52, no. 2, pp. 316–325, Feb. 2019, doi: 10.1021/acs.accounts.8b00516.

[13] G. Rizzello, P. Serafino, D. Naso, and S. Seelecke, "Towards Sensorless Soft Robotics: Self-Sensing Stiffness Control of Dielectric Elastomer Actuators," *IEEE Transactions on Robotics*, vol. 36, no. 1, pp. 174–188, 2020, doi: 10.1109/TRO.2019.2944592.

[14] O. A. Araromi *et al.*, "Rollable Multisegment Dielectric Elastomer Minimum Energy Structures for a Deployable Microsatellite Gripper," *IEEE/ASME Transactions on Mechatronics*, vol. 20, no. 1, pp. 438–446, 2015, doi: 10.1109/TMECH.2014.2329367.

[15] Z. Xing, J. Zhang, D. McCoul, Y. Cui, L. Sun, and J. Zhao, "A Super-Lightweight and Soft Manipulator Driven by Dielectric Elastomers.," *Soft Robot*, vol. 7, no. 4, Aug. 2020, doi: 10.1089/soro.2018.0134.

[16] J. Zhao, J. Zhang, D. McCoul, Y. Cui, and X. Lan, "A Soft Biomimetic Module of Elephant Trunk Driven by Dielectric Elastomers," in *2018 IEEE International Conference on Robotics and Biomimetics (ROBIO)*, 2018, pp. 349–354. doi: 10.1109/ROBIO.2018.8665147.

[17] M. Duduta, D. R. Clarke, and R. J. Wood, "A high speed soft robot based on dielectric elastomer actuators," in *2017 IEEE International Conference on Robotics and Automation (ICRA)*, 2017, pp. 4346–4351. doi: 10.1109/ICRA.2017.7989501.

[18] J. Shintake, V. Cacucciolo, H. Shea, and D. Floreano, “Soft Biomimetic Fish Robot Made of Dielectric Elastomer Actuators,” *Soft Robot*, vol. 5, no. 4, pp. 466–474, 2018, doi: 10.1089/soro.2017.0062.

[19] H. Godaba, J. Li, Y. Wang, and J. Zhu, “A Soft Jellyfish Robot Driven by a Dielectric Elastomer Actuator,” *IEEE Robot Autom Lett*, vol. 1, no. 2, pp. 624–631, 2016, doi: 10.1109/LRA.2016.2522498.

[20] G.-Y. Gu, J. Zhu, L.-M. Zhu, and X. Zhu, “A survey on dielectric elastomer actuators for soft robots,” *Bioinspiration &amp Biomimetics*, vol. 12, no. 1, p. 11003, Jan. 2017, doi: 10.1088/1748-3190/12/1/011003.

[21] S. Shian, J. Huang, S. Zhu, and D. R. Clarke, “Optimizing the Electrical Energy Conversion Cycle of Dielectric Elastomer Generators,” *Advanced Materials*, vol. 26, no. 38, pp. 6617–6621, 2014, doi: https://doi.org/10.1002/adma.201402291.

[22] Y. Chen, L. Agostini, G. Moretti, M. Fontana, and R. Vertechy, “Dielectric elastomer materials for large-strain actuation and energy harvesting: a comparison between styrenic rubber, natural rubber and acrylic elastomer,” *Smart Mater Struct*, vol. 28, no. 11, p. 114001, Oct. 2019, doi: 10.1088/1361-665x/ab3b32.

[23] J. Li, L. Liu, Y. Liu, and J. Leng, “Dielectric Elastomer Spring-Roll Bending Actuators: Applications in Soft Robotics and Design,” *Soft Robot*, vol. 6, no. 1, pp. 69–81, 2019, doi: 10.1089/soro.2018.0037.

[24] S. Michel, X. Zhang, M. Wissler, C. Löwe, and G. Kovacs, “A comparison between silicone and acrylic elastomers as dielectric materials in electroactive polymer actuators,” *Polym Int*, vol. 59, pp. 391–399, Mar. 2009, doi: 10.1002/pi.2751.

[25] Y. Chen, L. Agostini, G. Moretti, G. Berselli, M. Fontana, and R. Vertechy, “Fatigue life performances of silicone elastomer membranes for dielectric elastomer transducers: preliminary results,” in *Proc.SPIE*, Mar. 2019. doi: 10.1117/12.2515312.

[26] R. Kornbluh and R. Pelrine, “Chapter 4 - HIGH-PERFORMANCE ACRYLIC AND SILICONE ELASTOMERS,” in *Dielectric Elastomers as Electromechanical Transducers*, F. Carpi, D. De Rossi, R. Kornbluh, R. Pelrine, and P. Sommer-Larsen, Eds., Amsterdam: Elsevier, 2008, pp. 33–42. doi: https://doi.org/10.1016/B978-0-08-047488-5.00004-6.

[27] B. Fasolt, M. Hodgins, G. Rizzello, and S. Seelecke, “Effect of screen printing parameters on sensor and actuator performance of dielectric elastomer (DE) membranes,” *Sens Actuators A Phys*, vol. 265, pp. 10–19, Oct. 2017, doi: 10.1016/j.sna.2017.08.028.

[28] O. A. Araromi, A. T. Conn, C. S. Ling, J. M. Rossiter, R. Vaidyanathan, and S. C. Burgess, “Spray deposited multilayered dielectric elastomer actuators,” *Sens Actuators A Phys*, vol. 167, no. 2, pp. 459–467, 2011, doi: https://doi.org/10.1016/j.sna.2011.03.004.

[29] O. Araromi, S. Rosset, and H. Shea, “A deployable microsatellite gripper based on multi-segment dielectric elastomer actuators.”

[30] S. Nalbach, R. M. Banda, S. Croce, G. Rizzello, D. Naso, and S. Seelecke, “Modeling and Design Optimization of a Rotational Soft Robotic System Driven by Double Cone Dielectric Elastomer Actuators,” *Front Robot AI*, vol. 6, p. 150, 2020, doi: 10.3389/frobt.2019.00150.

[31] S. Hau, D. Bruch, G. Rizzello, P. Motzki, and S. Seelecke, “Silicone based dielectric elastomer strip actuators coupled with nonlinear biasing elements for large actuation strains,” *Smart Mater Struct*, vol. 27, no. 7, p. 74003, Jun. 2018, doi: 10.1088/1361-665x/aab7d8.

[32] P. Loew, G. Rizzello, and S. Seelecke, “A Novel Biasing Mechanism for Circular out-of-plane Dielectric Actuators Based on Permanent Magnets,” *Mechatronics*, vol. 56, pp. 48–57, Oct. 2018, doi: 10.1016/j.mechatronics.2018.10.005.

[33] J. Prechtl, J. Kunze, S. Seelecke, and G. Rizzello, “Soft Robotic Module Actuated by Silicone-Based Rolled Dielectric Elastomer Actuators - Modeling

and Simulation," in *ACTUATOR; International Conference and Exhibition on New Actuator Systems and Applications 2021*, 2021, pp. 1–4.

[34] J. Kunze *et al.*, "Design, Manufacturing, and Characterization of Thin, Core-Free, Rolled Dielectric Elastomer Actuators," *Actuators*, vol. 10, no. 4, 2021, doi: 10.3390/act10040069.

[35] J. Prechtl, J. Kunze, D. Bruch, S. Seelecke, and G. Rizzello, "Bistable Actuation in Multi-DoF Soft Robotic Modules Driven by Rolled Dielectric Elastomer Actuators," in *2021 IEEE 4th International Conference on Soft Robotics (RoboSoft)*, 2021, pp. 82–89. doi: 10.1109/RoboSoft51838.2021.9479246.

[36] E. Hajiesmaili and D. R. Clarke, "Dielectric elastomer actuators," *J Appl Phys*, vol. 129, no. 15, p. 151102, Apr. 2021, doi: 10.1063/5.0043959.

[37] G. Kovacs, L. Düring, S. Michel, and G. Terrasi, "Stacked dielectric elastomer actuator for tensile force transmission," *Sens Actuators A Phys*, vol. 155, no. 2, pp. 299–307, 2009, doi: https://doi.org/10.1016/j.sna.2009.08.027.

[38] N. Park and J. Kim, "Hydrogel-Based Artificial Muscles: Overview and Recent Progress," *Advanced Intelligent Systems*, vol. 2, no. 4, p. 1900135, 2020, doi: https://doi.org/10.1002/aisy.201900135.

[39] J. Prechtl, J. Kunze, G. Moretti, D. Bruch, S. Seelecke, and G. Rizzello, "Modeling and experimental validation of thin, tightly rolled dielectric elastomer actuators," *Smart Mater Struct*, vol. 31, no. 1, p. 15008, Nov. 2021, doi: 10.1088/1361-665x/ac34be.

[40] ultimaker, "Ultimaker-PETG-TDS-v1.00 Datasheet," https://support.ultimaker.com/hc/en-us/article_attachments/4777237744540/Ultimaker-PETG-TDS-v1.00.pdf.

[41] formlabs, "Rigid 10K Datasheet," https://formlabs-media.formlabs.com/datasheets/2001479-TDS-ENUS-0.pdf.

[42] D. Borzelli, S. Pastorelli, and L. Gastaldi, "Model of the human arm stiffness exerted by two antagoniste muscles," in *Advances in Intelligent Systems and Computing*, Springer Verlag, 2017, pp. 285–292. doi: 10.1007/978-3-319-49058-8_31.

2.3 Model-Based Synchronization of Dielectric Elastomers and Membrane Pumps for Performance-Optimized, Space-Efficient, and Application-Specific Pump Design

Hinweis zur Veröffentlichung:
Dieses Kapitel basiert auf folgendem begutachteten und zur Publikation angenommenen Artikel:

Autor(en): *M. Baltes* [a], *D. Bruch* [b], *P. Motzki* [a,b]

[a] Smart Material Systems, Center for Mechatronics and Automation Technologies (ZeMA gGmbH), Saarbrücken, Germany;

[b] Intelligent Material Systems Lab, Department of Systems Engineering, Department of Materials Science and Engineering, Saarland University, Saarbrücken, Germany

E-mail: matthias.baltes@imsl.uni-saarland.de, daniel.bruch@imsl.uni-saarland.de, paul.motzki@uni-saarland.de

Titel: Model-Based Synchronization of Dielectric Elastomers and Membrane Pumps for Performance-Optimized, Space-Efficient, and Application-Specific Pump Design.

Journal: Engineering Reports

DOI: http://dx.doi.org/10.1002/eng2.70237

Hinweis:

Supporting Information

S1. Fundamentals of Individual Components in DE-Based Pump Systems

A conventional pump consists of two main components: the pump mechanism and the drive system. In the case of a DE-based drive system, this in turn consists of two components: the DE and a biasing element. These three components will be examined in more detail in this section, and a selection of possible components for the design of the final system will be made based on the state of the art.

S1.1. Fundamentals of Dielectric Elastomers

Dielectric elastomers are a subgroup of electroactive polymers [22]. DEs are often likened to artificial muscles for their flexible structure, high energy density and efficiency, extensive deformability, rapid response, noiseless operation, and dual capability to actuate and sense (self-sensing) [23], [24], [25]. They consist of a thin elastomer film (e.g., silicone, acrylic, natural rubber) coated on both sides with flexible electrodes. The structure corresponds to the one of a parallel-plate capacitor, with the thin elastomer films as dielectric material [26]. When an electrical voltage is applied, the DE deforms due to his flexibility, a phenomenon utilized in building transducers. More detailed, during activation, the two electrodes of the DE are pulled together, due to the attractive electrical forces, causing the area to expand while simultaneously reducing its thickness (**Figure S1**). In this case, it is referred to as a dielectric elastomer actuator (DEA). Similarly, the capacitance can be measured to detect external deformations of the DE, making it suitable as a sensor. By combining these effects, a DEA can autonomously measure its own position without external sensors, a capability known as self-sensing [23], [24].

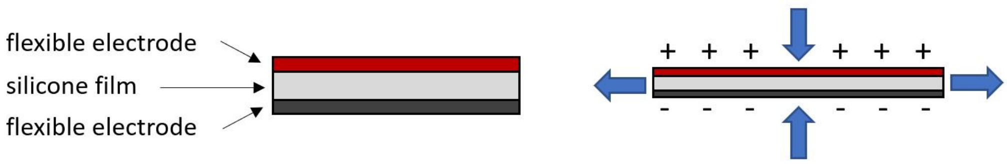

Figure S1. Working principle dielectric elastomer actuator

Two materials have established themselves as elastomers in the construction of DEs, including acrylic elastomers such as VHBTM 4910 and silicone (polydimethylsiloxane (PDMS)-based elastomers such as Elastosil 2030 15], [19], [20]. Both materials exhibit distinct characteristics that make them attractive for different applications. Acrylic elastomers can achieve large strains (up to 400-500%) with a low elastic modulus (around 20 kPa) [22], [26], [27]. However, they suffer from high mechanical losses and slow response times. This makes them suitable for numerous applications in the field of soft robotics [28], [29]. If prioritizing fast response time over high deformation, silicone-based DEs are advantageous. While they offer a smaller deformation capability of around 100%, they are approximately 50 times faster [26], [30]. Another advantage, particularly valuable for product-oriented applications, is their longevity, which is about 100 times longer [26]. Therefore, silicone-based actuators are used in applications where high actuation frequency is required, such as loudspeakers, haptic devices and pumps [20]. To avoid limiting the system to low operating frequencies, the focus will be on silicone-based actuators in the following sections.

Electrodes, consisting of carbon black particles suspended in a mixture of PDMS, are screen printed on the silicone film to manufacture the finished DE [25]. Screen printing allows to produce a wide variety of geometries for the electrodes, and consequently for the DE as well. In addition to a variety of flexible custom designs, three standard geometries that utilize the planar surface expansion effect for transduction have become particularly well-established. The SIP-DE (strip-in-plane-DE) has a rectangular shape and deforms in-plane upon activation [30]. A modified form is the rolled dielectric elastomer (RDE), where from the principle, a SIP is rolled up into a cylindrical shape [29], [31]. As a third geometry, the COP-DE (circular out-ofplane DE) is a circular DE that, when actuated, deflects out of plane like a speaker membrane [11], [32]. The SIP and RDE differ mainly in their spatial configuration but vary in their operational mode and force-displacement characteristics (**Figure S2**). In contrast, the COP exhibits a different force-displacement-characteristic due to its out-of-plane actuation. This characteristic can be tailored to the specific application in both cases by adjusting the geometry of the DE.

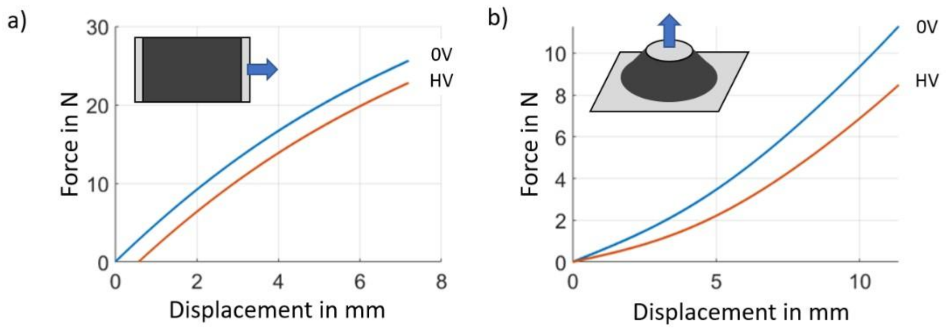

Figure S2. Force displacement characteristic SIP-DEs (a) and COP-DEs (b)

When restricted by spatial constraints, the force can be scaled by parallel connection of multiple DEAs. For COPs and SIPs, multiple individual DEs can be stacked to achieve this [33]. The force adds up in this case through the principle of superposition. In the case of the pump, we will focus on the COP design for the DEs. Due to their membrane structure, they are highly compatible in terms of spatial integration with membrane pumps, which will be discussed in more detail in Chapter 3. Additionally, their inherent structure lacks open edges, which improves handling and enhances robustness against external influences such as contamination. To utilize the area expansion of the DE effectively in building a transducer that generates a specific force and stroke behavior, the DE must be coupled with a biasing mechanism. These mechanisms will be detailed in the next section.

S1.2. Fundamentals of Biasing Elements

As biasing mechanisms, various mechanical components (e.g mass, linear spring, permanent magnet, negative-rate bias spring) can be used that exhibit a specific force-displacement characteristic, counteracting the DE and thus guiding it in the desired direction when electrical voltage is applied [32], [34], [35].An actuator for static operation can be adapted to a specific load force or force profile based on the characteristic curves of its biasing mechanism and its DE-element. In pumps, which are often operated dynamically, dynamic effects occur. Therefore, the resulting forces must also be taken into account. . Here, the properties of all the components must be incorporated into the system equations, which are later used to simulate the system. In the case of the pump, it is important to be able to freely vary the stiffness of the system to leverage resonance effects and thereby increase the system's efficiency. To keep this as general as possible, we consider both negative and positive constant stiffness values. Positive stiffness can be easily achieved by selecting an appropriate linear spring. Negative stiffness can be specifically generated through the design of a buckled beam and its parameters [21], [30]. The buckled beam design has to be chosen to ensure that the system always operates within the range of constant negative stiffness.

By coupling the DE with a biasing element, an actuator capable of performing specific mechanical work can be created. To develop the complete pump system, the pump mechanism needs to be examined in detail next. This mechanism determines the work, stroke, and force required from the actuator to achieve the desired pump characteristics, such as flow rate and pressure.

S1.3. Fundamentals of Pump Mechanisms

Pump mechanisms can be categorized based on their required actuation direction. In the case of DE-based transducers that generate linear motion, pumps with rotational drives involve additional mechanical components and losses and therefore will not be considered further. Piston pumps and diaphragm pumps are the two most commonly used pump mechanisms based on linear motion. Both mechanisms operate by compressing a volume through linear motion and directing the pump medium/fluid through an outlet valve. Upon retracting, the volume increases again, allowing new fluid to be drawn in through an inlet valve for pumping. In the case of a piston pump, the volume is compressed by a piston, similar to an internal combustion engine. In contrast, a diaphragm pump compresses the volume using a deformable but nonstretchable membrane. For small, lightweight applications, diaphragm pumps are advantageous [4]. For applications requiring higher pressures, piston pumps are preferred because they can withstand the higher forces resulting from the pressure [8]. In everyday applications, diaphragm pumps are often sufficient. Therefore, these pumps are the focus of this work and will be examined in detail.

Diaphragm pumps consist of three main components: the pump chamber, which provides the basic structure for compressing the fluid volume; the pump membrane, which compresses the fluid from its initial to target volume; and the valves, which direct the flow of fluid in a controlled manner. The combination of the pump chamber and membrane defines the maximum volume V_{max} of fluid that can be contained within the pump chamber. At the maximum stroke d_{max} of the pump membrane, the chamber holds the minimum volume V_{min}. The ratio of these two volumes, multiplied by the ambient pressure $p_{ambient}$ at the inlet valve, describes the maximum/minimum pressure (p_{max} / p_{min}) that this pump can generate. It is important to distinguish between vacuum pumps and pumps that generate overpressure. In overpressure pumps, the pressure tank or the component where pressure is to be generated is connected at the outlet valve. In vacuum pumps it is connected at the inlet valve, generating a pressure lower than the ambient pressure. With Boyle's and Mariotte's law, the formulas (S1,S2) for the differential pressure achievable directly derived.

vacuum pump: $$p_{min} = p_{ambient}\frac{V_{min}}{V_{max}} \tag{S1}$$

overpressure pump: $$p_{max} = p_{ambient}\frac{V_{max}}{V_{min}} \tag{S2}$$

For the pump membrane itself, there are various approaches. Rubber membranes can be used, which roll or fold together to reduce the volume [36], [37]. Alternatively, as shown in **Figure S3** a bi-stable membrane made from a robust material can be used. This type of membrane is stable in both the minimum and maximum deflection positions and can snap between these positions. The geometry of the membrane and the pump chamber determines the maximum achievable pressure of the pump. The second crucial parameter of the pump also depends partly on these two components. The maximum volume that can be delivered per cycle is the difference between V_{max} and V_{min}. This, along with the operating frequency f_{op} of the pump, determines the free flow rate q_{free}.

$$q_{free} = f_{op}(V_{max} - V_{min}) \tag{S3}$$

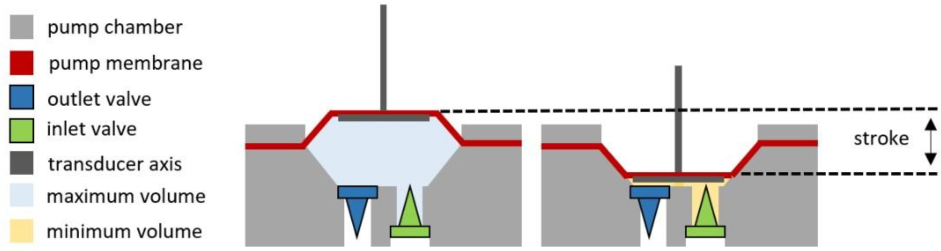

Figure S3. Working principle diaphragm pumps

The flow is directed by the check valves, which can include various types of passive valves such as flap/membrane valves or duckbill valves for applications with smaller differential pressures, and ball valves for high-pressure applications. How the individual components and their geometries affect the force-displacement characteristics will be examined in the next chapter. Here, the components required to formulate the system equation for the pump will be designed.

S2. Component design and manufacturing

To demonstrate an application-oriented design approach, this process is exemplified through the design of an industry-suitable pump. Specifically, a vacuum pump is designed to achieve a minimum absolute pressure of 300 mbar and a free flow rate of 0.5 l/min. As a spatial constraint, the pump's footprint is limited to 45x45 mm. By adhering to these specifications, the design process is guided by real-world requirements, ensuring the pump meets industrial standards while fitting within the given space restrictions. The interplay between performance goals and dimensional limitations drives the optimization of design parameters, resulting in a technically feasible solution.

In this section, the first two components of the pump required to meet the targeted specifications are designed and manufactured. The process begins with designing the pump chamber to ensure maximum pressure and free flow. Subsequently, a DE element is tailored to fit this pump chamber, with its geometry adjusted to support the chamber's functionality effectively.

S2.1 Pump chamber design and manufacturing

The design of the pump chamber is primarily determined by two critical requirements: the maximum differential pressure to be achieved and the free flow rate. As described in section S1.3, the ratio between the initial volume and the maximally compressed volume of the pump chamber determines the maximum achievable differential pressure (S1), (S2). The volume difference, together with the operating frequency, defines the free flow rate (S3). However, these two criteria alone are insufficient to fully define the design. To determine an optimal geometry, the ratio between the chamber cross-section and the stroke of the pump membrane plays a crucial role. The stroke, in turn, must match the actuator element, which in our case is the DE. Based on the specified installation space requirements and comparable COP-DEs, a stroke of 3 mm is selected, as this is a realistic value that can be implemented within this space using DEs. The target pressure is 300 mbar absolute, meaning the initial volume inside the pump chamber must be compressed by 70%, this ensures that during the expansion phase, a negative pressure is generated, which, in the maximum case, leads to a pressure equilibrium of 300 mBar within the chamber and the pressure tank. Considering the unknown dead volume in the valves and connecting lines, a higher compression ratio of 80% is employed to ensure the target pressure is reached. This over-compression provides a margin for fine-tuning the system. By subsequently reducing the actuation amplitude (via lowering the actuation voltage), the operating point where the pump exactly achieves 300 mbar can be precisely adjusted. For straightforward modeling and specifications-oriented design, a cylindrical geometry for the chamber would be suitable. This assumption will be maintained for calculations. A purely cylindrical shape, however, is not optimal in practice, as the pump membrane must deflect into the cylinder, requiring it to be highly flexible, which conflicts with the need for pressure resistance. High flexibility would typically reduce the membrane's ability to withstand pressure, leading to a trade-off between flexibility and structural integrity. If the membrane itself has a cylindrical shape, it would need to fully fold into the cylinder, leading to significant mechanical stress between the two extreme positions. This issue can be mitigated by using a nearly cylindrical truncated cone (frustum) for the chamber and the pump membrane. The pump membrane can be designed to be bistable, allowing it to fully collapse into the conical chamber. **Figure S4** illustrates the cross-section of the chamber with the pump membrane and its cylindrical simplification. The maximum stroke between the two bi-stable positions of the pump membrane corresponds to the previously defined 3 mm. In the cylindrical simplification, the initial chamber volume V_{max} is compressed by 80% to V_{min}. By optimizing the angle of the truncated cone, the membrane can transition smoothly between positions with reduced stress. Importantly, a steep angle for the conical section ensures that the force-displacement characteristics of the system can still be approximated using the cylindrical simplification for computational purposes.

Based on the previously established design requirements, the pump chamber is constructed with the geometry depicted in **Figure S4**.

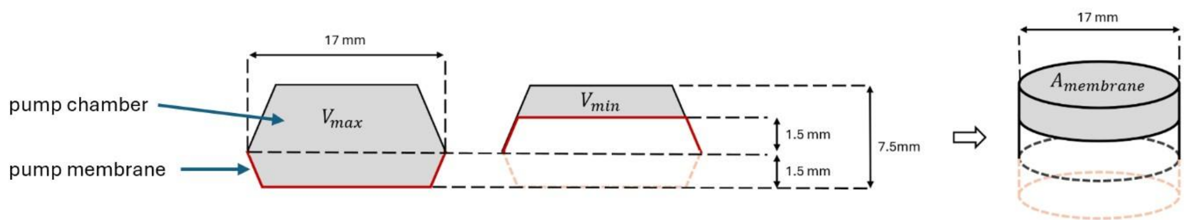

Figure S4: Pump chamber geometry and its simplification

In addition to pressure, the free flow also plays a crucial role. This can later be adjusted based on the differential volume and the operating frequency for optimal performance. The resonance frequency can be selected by adjusting the system stiffness, ensuring that the pump generates the desired flow at this operating frequency. The chamber itself is fabricated using clear resin from Formlabs via 3D printing. This material is chosen for its impermeability and smooth surface finish, which ensures a tight seal with the pump membrane [38]. The valves, in this case, duckbill valves, can also be self-sealing and directly integrated into the 3D printed housing as needed. The pump membrane must be flexible but not stretchable, and therefore, an FEP (fluorinated ethylene propylene) film is employed. The ability of the membrane to fold into the pump chamber and maintain a stable geometry during operation is achieved through its bistable design. This bi-stability allows the membrane to operate in two distinct stable states: one where it is fully extended, and another where it is folded into the chamber. Through a thermoforming process, the desired geometry of the membrane can be precisely created. In this process, the FEP film is heated until it becomes pliable and is then shaped into the required form using a mold. As the film cools, it retains the newly formed geometry. Several film thicknesses, ranging from 50 μm to 200 μm, are tested. In order to reduce the intrinsic force of the membrane, the thinnest possible option is chosen. However, thicknesses below 100 μm have shown that after several tests, the membrane gets damaged and tears at the connection point to the shaft. The membrane is attached to the pump chamber using a clamping connection. To ensure a proper seal, a silicone gasket is placed between the lower part of the chamber and the membrane. The individual components of the pump chamber are shown in **Figure S5**.

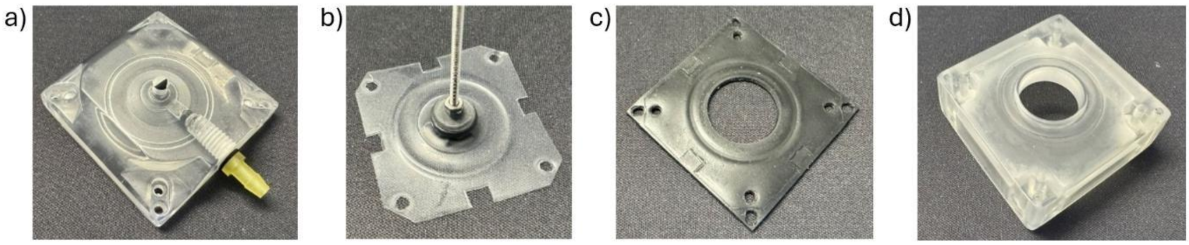

Figure S5. Pump chamber components: a) the upper housing half with valves, b) the FEP pump membrane, c) the silicone gasket, and d) the lower housing half.

Based on the maximum stroke of the pump chamber of 3 mm and the installation space requirements, a DE element can be designed and manufactured in the next step.

S2.2 DE-element design and manufacturing

As a basic DE design, the focus will be on COP-DEs. These are chosen because they can be mounted parallel to the pump membrane. Since COP-DEs themselves have a membrane structure, they complement each other in operation and can be installed in a space-saving manner. As design parameters for COP-DEs, the outer radius and inner radius are crucial factors. As described in Section S1, the force generated by the DE can be scaled by stacking multiple DEs on top of each other. Generally, a larger outer radius results in greater force generated by the DE. Moreover, increasing the ratio of outer to inner radius enhances the maximum possible displacement while reducing stiffness and slightly the maximum achievable force of the actuator [39]. When developing an optimized pump for specific applications, spatial constraints often dictate the design. To maximize the performance of the DE, its geometry is tailored to fit within these constraints. The outer radius is chosen as large as possible to fit within the space limitations, considering clamping and other necessary components. The inner radius is then selected to achieve a target stroke planned for the pump chamber design, while ensuring the electric field remains within limits to guarantee the DEs longevity. Further optimization of the system is achieved by selecting the appropriate number of layers n_{DE}. In this work, to validate the methodology, a DE is designed precisely according to these requirements for a specific spatial constraint. Subsequently, it is experimentally characterized. The pre-strain of the DE

($x_{0\ DE}$) and the stacked amount of DEs (n_{DE}) then serve as design parameters for the pump. The exact parameters will be determined through measurements after constructing the initial DE element in the next section.

With a footprint of 45 mm x 45 mm, an electrode diameter of 39 mm is chosen, leaving 2.5 mm per side for clamping the silicone films and a 0.5 mm gap between the electrode and the clamp to prevent the electrode from being damaged. The clamp consists of two frames made of Formlabs Rigid 10k material [40], each with a thickness of 1.75 mm. These frames feature a tongue and groove design, which securely holds the individual silicone films in place. The frames are connected using melt rivets. An inner radius of 17 mm is chosen, providing sufficient space for securing the motion axis and riveting the two clamps. The inner radius primarily affects the stiffness of the DE; however, this can later be compensated by the biasing mechanism. Therefore, priority is given to ensuring ease of handling at this stage. In a single DE stack (**Figure S6**), 17 silicone films, each printed with an electrode on one side, are stacked to create a 16-layer DE stack. Theoretically, more layers are possible; however, experiments have shown that for higher resulting forces, the thickness of the frames must be adjusted. A 16-layer stack, with a height of around 4 mm, has proven to be practical and robust. With a voltage of 2300 V, the DE can thus be deflected up to 10 mm while keeping the electric field below 80 V/µm. This provides a good working range, offering design flexibility for the pump chamber with stroke ranges up to 3 mm (suitable and save working range between 6mm and 9mm). The design parameters for the DEs have thus been restricted to the number of layers, while size and layout have been chosen to maximize the work output within the given spatial constraints. This ensures that the total number of DEs remains minimal, while still achieving an optimal design for the available footprint. By focusing on maximizing the efficiency of the DEs within the limited space, the design minimizes material use and complexity, while maintaining high performance, ensuring that the pump operates effectively within the defined geometric boundaries.

Figure S6. Mechanical structure single DE-element

In the next chapter, the two components manufactured in this chapter are experimentally characterized. This serves both to validate the required specifications and, furthermore, the experiments provide the basis for generating the models needed to establish the equation of motion.

S3 Component characterization

To establish the equation of motion, the force-displacement characteristics of the individual components are required. For the pump chamber, this characteristic depends on the load pressure, and for the DEs, it depends on the applied electrical voltage. Experiments are conducted to investigate these dependencies, allowing the models to be validated and unknown parameters to be determined.

S3.1 Pump chamber characterization

The overall force-displacement characteristic of the pump chamber depends on two different components. On the one hand, the force generated by the stiffness of the pump membrane, and on the other hand, the force exerted by the load pressure applied to the surface of the pump membrane. In our case, the load pressure varies from ambient pressure to the minimum possible absolute pressure that the pump chamber can generate. The target pressure is 300 mbar absolute pressure. To determine all the required information for the previously manufactured pump chamber, two experiments are conducted. In the first experiment, a closed volume is connected to the inlet valve of the pump chamber. The pump membrane is actuated reciprocally using a linear actuator. By simultaneously measuring the load pressure and the membrane force, the pressure-dependent load force of the pump chamber can be determined. Additionally, these measurements can verify whether the desired target pressure is achievable with the chosen pump design. The experimental setup is schematically illustrated in **Figure S7**.

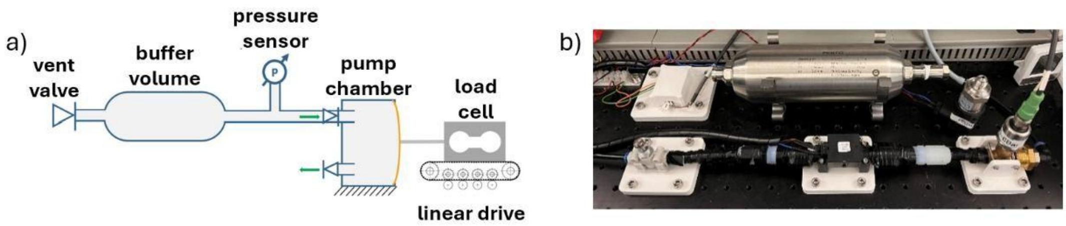

Figure S7. a) the schematic experimental setup for characterizing the pump chamber and b) the actual setup.

To determine the membrane force, the setup can be slightly modified in a second experiment: the outlet valve must simply be removed. In this configuration, the pump performs no work, the membrane is subjected to ambient pressure, and the pure force arising from the membrane's stiffness can be measured.

In **Figure S8**, the force characteristics of the pump chamber and pump membrane are shown on the left, while the load force of the pump chamber with the corresponding pressure is depicted on the right. In the first step, it is immediately noticeable that the load force of the pump membrane is relatively small compared to the load force generated by the pressure and therefore can be neglected in the following analysis. The right plot also clearly shows the maximum achievable pressure, which reaches approximately 260 mbar. Although the pump does not reach the expected 200 mbar pressure at 80% compression, it performs better than the desired target pressure of 300 mbar. The 60 mbar difference from the theoretically planned result can be explained by the previously mentioned dead volume, which was not accounted for, arising from the valves and their installation space.

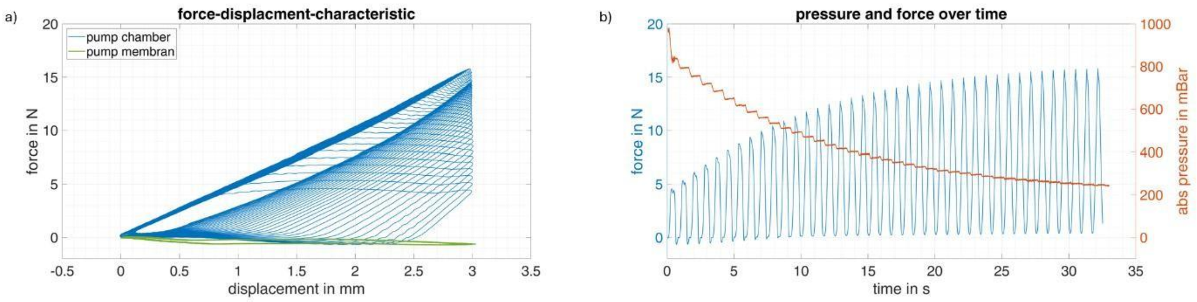

Figure S8. Force characteristic of the individual pump chamber components (a) in relation to the corresponding load pressure (b).

S3.2 DE-element characterization

In the next step, the DE element is experimentally investigated to determine its necessary characteristics for solving the equation of motion. This experimental analysis will provide key parameters, such as stiffness and voltage dependency, which are essential for accurately modeling the system dynamics. By obtaining these specific characteristics, the DE's behavior under operating conditions can be precisely incorporated into the equation, allowing for a more reliable and optimized solution to the motion equation. To characterize the DE-element, two sets of measurements are taken: the force-displacement behavior is first recorded for a displacement range of 0–10 mm without any applied external voltage, and then under the application of 2300 V. The voltage of 2300 V is chosen to ensure the DE is subjected to a maximum electric field of 70 V/µm. This value corresponds to approximately 80% of the maximum electric field tested during the manufacturing process (90 V/µm), which is intentionally reduced to prolong the DE's operational lifespan through multiple cycles, by minimizing the risk of electrical breakthroughs. **Figure S9** illustrates the schematic measurement setup for the electromechanical characterization of a DE and the two-resulting force-displacement curves.

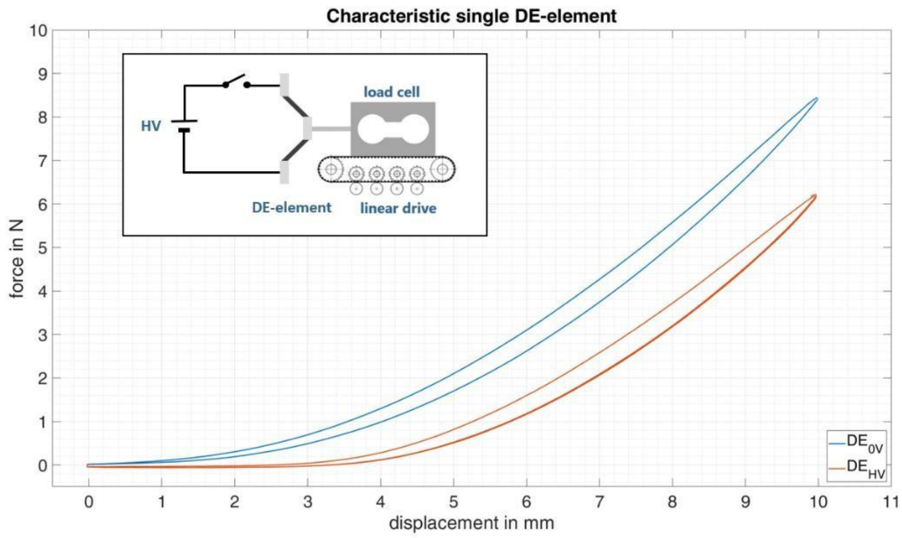

Figure S9. Force-displacement-characteristic 16 layer DE-element

These characteristic curves are used in the subsequent chapter to create a numerical model. What can be directly validated here, however, is the operating range. This is planned for a 3 mm stroke of the pump membrane, and the range between 6 mm and 9 mm allows for a large operating range with a relatively small electric field of under 70V/µm, ensuring safe and DE-friendly operation.

References

[25] M. Hodgins and S. Seelecke, "Mechanical Behavior of a Bi-Stable Negative-Rate Bias Spring System," *Proceedings of SPIE - The International Society for Optical Engineering*, vol. 7644, Mar. 2010, doi: 10.1117/12.852373.

[26] R. Kornbluh and R. Pelrine, "Chapter 4 - HIGH-PERFORMANCE ACRYLIC AND SILICONE ELASTOMERS," in *Dielectric Elastomers as Electromechanical Transducers*, F. Carpi, D. De Rossi, R. Kornbluh, R. Pelrine, and P. Sommer-Larsen, Eds., Amsterdam: Elsevier, 2008, pp. 33–42. doi: https://doi.org/10.1016/B978-0-08-047488-5.00004-6.

[27] G. Rizzello, P. Serafino, D. Naso, and S. Seelecke, “Towards Sensorless Soft Robotics: Self-Sensing Stiffness Control of Dielectric Elastomer Actuators,” *IEEE Transactions on Robotics*, vol. 36, no. 1, pp. 174–188, 2020, doi: 10.1109/TRO.2019.2944592.

[28] N. Ni and L. Zhang, “Dielectric Elastomer Sensors,” 2017. doi: 10.5772/intechopen.68995.

[29] B. Fasolt, M. Hodgins, G. Rizzello, and S. Seelecke, “Effect of screen printing parameters on sensor and actuator performance of dielectric elastomer (DE) membranes,” *Sens Actuators A Phys*, vol. 265, pp. 10–19, Oct. 2017, doi: 10.1016/j.sna.2017.08.028.

[30] S. Michel, X. Zhang, M. Wissler, C. Löwe, and G. Kovacs, “A comparison between silicone and acrylic elastomers as dielectric materials in electroactive polymer actuators,” *Polym Int*, vol. 59, pp. 391–399, Mar. 2009, doi: 10.1002/pi.2751.

[31] Y. Chen, L. Agostini, G. Moretti, M. Fontana, and R. Vertechy, “Dielectric elastomer materials for large-strain actuation and energy harvesting: a comparison between styrenic rubber, natural rubber and acrylic elastomer,” *Smart Mater Struct*, vol. 28, no. 11, p. 114001, Oct. 2019, doi: 10.1088/1361-665x/ab3b32.

[32] J. Prechtl, J. Kunze, S. Seelecke, and G. Rizzello, “Soft Robotic Module Actuated by Silicone-Based Rolled Dielectric Elastomer Actuators - Modeling and Simulation,” in *ACTUATOR; International Conference and Exhibition on New Actuator Systems and Applications 2021*, 2021, pp. 1–4.

[33] J. Kunze *et al.*, “Design and fabrication of silicone-based dielectric elastomer rolled actuators for soft robotic applications,” Oct. 2020, p. 80. doi: 10.1117/12.2558444.

[34] S. Hau, D. Bruch, G. Rizzello, P. Motzki, and S. Seelecke, “Silicone based dielectric elastomer strip actuators coupled with nonlinear biasing elements for large actuation strains,” *Smart Mater Struct*, vol. 27, no. 7, p. 74003, Jun. 2018, doi: 10.1088/1361-665x/aab7d8.

[35] J. Prechtl, J. Kunze, G. Moretti, D. Bruch, S. Seelecke, and G. Rizzello, “Modeling and experimental validation of thin, tightly rolled dielectric elastomer actuators,” *Smart Mater Struct*, vol. 31, no. 1, p. 15008, Nov. 2021, doi: 10.1088/1361-665x/ac34be.

[36] P. Loew, G. Rizzello, and S. Seelecke, “A Novel Biasing Mechanism for Circular out-of-plane Dielectric Actuators Based on Permanent Magnets,” *Mechatronics*, vol. 56, pp. 48–57, Oct. 2018, doi: 10.1016/j.mechatronics.2018.10.005.

[37] G. Kovacs, L. Düring, S. Michel, and G. Terrasi, “Stacked dielectric elastomer actuator for tensile force transmission,” *Sens Actuators A Phys*, vol. 155, no. 2, pp. 299–307, 2009, doi: https://doi.org/10.1016/j.sna.2009.08.027.

[38] M. Hodgins, A. York, and S. Seelecke, “Experimental comparison of bias elements for out-of-plane DEAP actuator system,” *Smart Mater Struct*, vol. 22, no. 9, p. 094016, 2013, doi: 10.1088/0964-1726/22/9/094016.

[39] J. Neu, J. Hubertus, S. Croce, G. Schultes, S. Seelecke, and G. Rizzello, “Fully Polymeric Domes as High-Stroke Biasing System for Soft Dielectric Elastomer Actuators,” *Front Robot AI*, vol. 8, p. 171, 2021, doi: 10.3389/frobt.2021.695918.

[40] G. Mimmi and P. Pennacchi, “Diaphragm design improvement for a metering pump,” *Eng Fail Anal*, vol. 8, no. 1, pp. 1–13, 2001, doi: https://doi.org/10.1016/S1350-6307(00)00007-8.

[41] E. Meng, X.-Q. Wang, H. Mak, and Y.-C. Tai, “A check-valved silicone diaphragm pump,” in *Proceedings IEEE Thirteenth Annual International Conference on Micro Electro Mechanical Systems (Cat. No.00CH36308)*, 2000, pp. 62–67. doi: 10.1109/MEMSYS.2000.838491.

[42] formlabs, “Standard Materials for High-Resolution Rapid Prototyping.” Accessed: Jan. 08, 2025. [Online]. Available: https://formlabs-media.formlabs.com/datasheets/Clear_Resin_Technical.pdf

[43] S. Hau, A. York, G. Rizzello, and S. Seelecke, “Performance Prediction and Scaling Laws of Circular Dielectric Elastomer Membrane Actuators,” *Journal of Mechanical Design*, vol. 140, no. 11, Nov. 2018, doi: 10.1115/1.4039104.

[44] formlabs, “Rigid 10K Datasheet,” https://formlabs-media.formlabs.com/datasheets/2001479-TDS-ENUS-0.pdf.

2.4 Electronic Control System for Optimized Resonance Operation of Dielectric Elastomer Pumps Through Self-Sensing

Hinweis zur Veröffentlichung:
Dieses Kapitel basiert auf folgendem begutachteten und zur Publikation angenommenen Artikel:

Autor(en): Matthias Baltes[a], Benedikt Holz[b], Daniel Bruch[b], Paul Motzki[a,b]

[a] Smart Material Systems, Center for Mechatronics and Automation Technologies (ZeMA gGmbH), Saarbrücken, Germany;

[b] Intelligent Material Systems Lab, Department of Systems Engineering, Department of Materials Science and Engineering, Saarland University, Saarbrücken, Germany

E-mail: matthias.baltes@imsl.uni-saarland.de, benedikt.holz@imsl.uni-saarland.de, daniel.bruch@imsl.uni-saarland.de, paul.motzki@uni-saarland.de

Titel: Model-Based Synchronization of Dielectric Elastomers and Membrane Pumps for Performance-Optimized, Space-Efficient, and Application-Specific Pump Design.

Journal: Advanced Engineering Materials

DOI: https://doi.org/10.1002/adem.202501204

Supporting Information

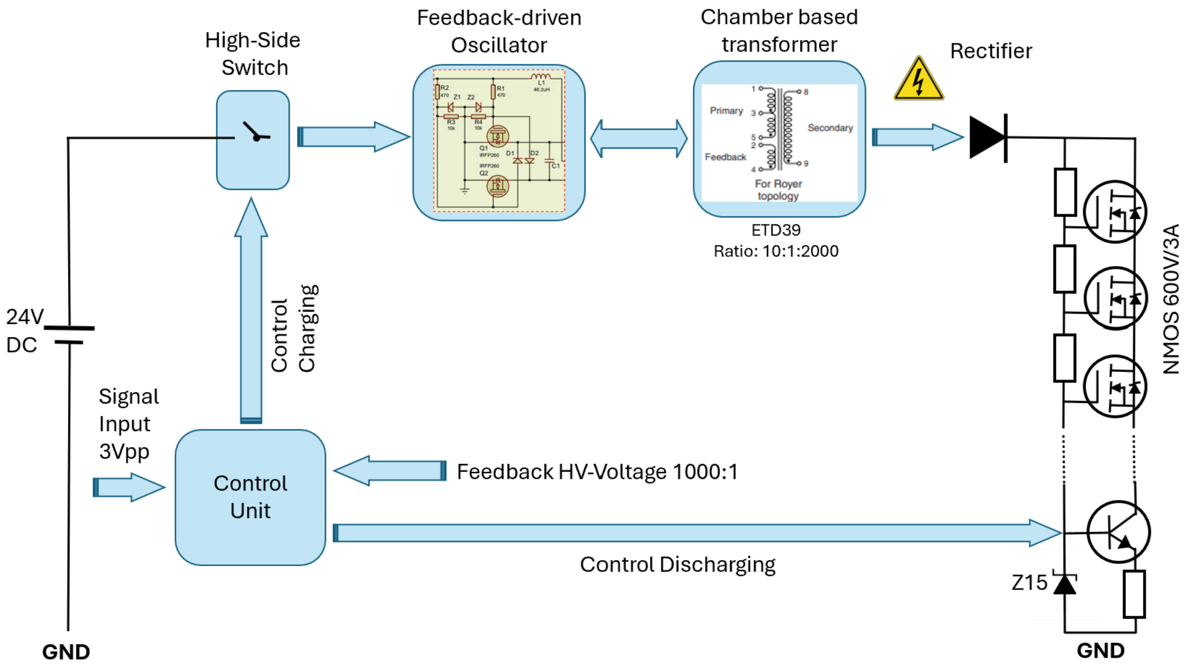

S1 electronic circuit concept

Fazit und Ausblick

Übergeordnete Leitfrage (Rahmen der Dissertation):

1. *Inwiefern können dielektrische Elastomer-Aktoren (DE-Aktoren) durch intelligente Auslegung, Fortschritte in der Herstellung, Design und Systemintegration weiterentwickelt werden, dass sie eine realistische, wettbewerbsfähige Alternative zu etablierten Aktorsystemen darstellen?*

In den drei vorliegenden Veröffentlichungen wurden vielversprechende Ansätze zur Weiterentwicklung von DE-Aktoren vorgestellt. Insbesondere konnte an zwei konkreten Beispielen gezeigt werden, wie diese neu entwickelten Konzepte so ausgelegt werden können, dass sie den Anforderungen verschiedener Anwendungsbereiche gerecht werden. Dadurch eröffnen sich neue Einsatzmöglichkeiten im Alltag und zukünftigen relevanten Anwendungsfeldern, etwa im Bereich der Softrobotik, wo die Flexibilität und Anpassungsfähigkeit der DE-Aktoren besonders zum Tragen kommen. Darüber hinaus sind die entwickelten Ansätze geeignet, konventionelle Antriebssysteme, beispielsweise für Pumpen, zu ersetzen.

Die Ergebnisse belegen dabei eindrucksvoll, dass durch intelligente Auslegung, optimierte Herstellungsprozesse sowie fortschrittliche Systemintegration das Potenzial besteht, DE-Aktoren als realistische und wettbewerbsfähige Alternative zu etablierten Aktor Systemen einzusetzen. Dabei wurde nicht nur der Fokus auf die funktionale Leistungsfähigkeit gelegt, sondern auch auf Aspekte wie Skalierbarkeit, Energieeffizienz und die Integration smarter Funktionen, die klassische Technologien an ihre Grenzen bringen.

Material & Herstellung (Grundlage für alle Anwendungen):

2. *Kann der Herstellungsprozess von DE-Aktoren mit Hinblick auf reproduzierbare Qualität, hohe Dauerfestigkeit und Skalierbarkeit für die Massenproduktion weiterentwickelt werden?*

Es wurden zwei verschiedene Ansätze zur Skalierbarkeit und Qualitätssicherung bei der Herstellung der DE-Aktoren demonstriert. Am Beispiel der Softrobotik wurden speziell optimierte RDEAs entwickelt. Hierbei kam, analog zu den COPs der Pumpe, ein gezielter Reparaturprozess der Elastomerfilme nach dem Aufbringen der Elektroden zum Einsatz, um den Ausschuss signifikant zu verringern.

Sowohl beim Rollprozess der RDEAs als auch beim Stapelprozess der COPs wurde bei der Materialauswahl und den Fertigungsschritten konsequent darauf geachtet, skalierbare und reproduzierbare Prozesse umzusetzen. Obwohl die Fertigung in der vorliegenden Arbeit noch händisch durchgeführt wurde, wurden sämtliche

Prozessschritte so gestaltet, dass sie sich prinzipiell teil- oder vollständig automatisieren lassen. Damit wurde eine wesentliche Grundlage geschaffen, um die DE-Aktoren nicht nur in der Einzelanfertigung, sondern perspektivisch auch in einer kosteneffizienten Serienproduktion herzustellen.

Mehrdimensionale Bewegungen (Soft-Robotik):

3. *Inwieweit lassen sich bistabile Konzepte, die bisher für eindimensionale DE-Aktoren genutzt wurden, auf mehrdimensionale Systeme übertragen, um große Hübe zu realisieren?*
4. *Können Silikon-basierte DE-Aktoren Aktorhübe erreichen, die mit VHB-basierten Systemen vergleichbar sind und gleichzeitig verbesserte Reaktionszeiten in Soft-Robotik-Strukturen realisieren?*

Im Bereich der Softrobotik wurde in dieser Arbeit der bestehende Stand der Technik signifikant erweitert. Während sich silikonbasierte Module bislang typischerweise auf Biegewinkel von etwa 10° beschränkten oder VHB-basierte Module aufgrund ihrer sehr langen Reaktionszeiten nur eingeschränkt einsetzbar waren, konnte hier ein neuartiges Softrobotik-Modul entwickelt werden, das diese Limitationen überwindet. Das entwickelte System erreicht Biegewinkel von bis zu 25° in beide Richtungen und zeichnet sich gleichzeitig durch eine deutlich reduzierte Reaktionszeit von unter einer Sekunde aus. Ein erheblicher Fortschritt im Vergleich zu den minutenlangen Ansprechzeiten klassischer VHB-basierter Systeme.

Ermöglicht wurde dieser Fortschritt durch die gezielte Adaption eines Aktorkonzepts aus dem eindimensionalen Bereich. Durch die Integration eines elastischen Backbones wurde ein bistabiles System für zweidimensionale Bewegungen realisiert, bei dem gezielt zwischen den beiden stabilen Positionen umgeschaltet werden kann. Diese Architektur erlaubt nicht nur große, schnelle Bewegungen, sondern bildet auch die Grundlage für zukünftige Erweiterungen in den dreidimensionalen Raum.

Ein weiteres großes Potenzial für die Weiterentwicklung dieses Ansatzes liegt im Einsatz von Self-Sensing-Technologien. Erste Ansätze dazu wurden bereits umgesetzt [13], [56], [57], um die aktuelle Position des Moduls zu erfassen. Zukünftige Arbeiten können auf diesem Konzept aufbauen, um jede beliebige Zwischenposition zwischen den beiden maximalen Auslenkungen gezielt anzusteuern, präzise zu regeln und stabil zu halten. Für die aktuell noch vergleichsweise geringe Kraft des Moduls bietet sich ein Konzept an, das durch das Bündeln mehrerer RDEAs, analog zur Strukturierung von Muskelfasern, eine Kraftskalierung ermöglicht. Dieses biologische Vorbild wird im Rahmen zukünftiger Forschungsarbeiten weiter untersucht, um die Einsatzmöglichkeiten des Softrobotik-Systems signifikant zu erweitern.

Dynamische Bewegungen (Pumpen):

5. *Lassen sich Antriebssysteme auf DEA Basis in Leistungsdichte und Antriebsleistung entwickeln um konventionelle Pumpenantriebe zu ersetzen?*
6. *Wie kann das Gesamtsystem, bestehend aus DE-Aktor, Pumpenstruktur und Last, modellbasiert und simulationsgestützt so ausgelegt werden, dass die Energieeffizienz maximiert und die Betriebsweise optimiert wird?*
7. *Wie kann der Self-Sensing-Effekt von DEs in Verbindung mit kompakter, kosteneffizienter Elektronik genutzt werden, um relevante Systemkenngrößen (z. B. Druck, Auslenkung) präzise zu erfassen und zu überwachen?*
8. *In welchem Maße lässt sich durch die Integration von Self-Sensing und intelligenter Ansteuerungselektronik ein autonomes, adaptives Pumpensystem realisieren, das herkömmlichen Pumpen überlegen ist?*

Im Bereich dynamischer Anwendungen wurde systematisch eine Pumpe entwickelt, die auf den Anforderungen konventioneller Vakuumpumpen hinsichtlich Druck, Durchfluss und Bauraum basiert. Anhand dieser Vorgaben wurde das Gesamtsystem modelliert und mittels Simulationen optimiert. Dabei lag der Fokus insbesondere auf der Abstimmung von Arbeitsfrequenz und Resonanzfrequenz, um die Pumpe für die veränderliche Last dynamisch zu optimieren. In iterativen Fertigungsschritten wurden die einzelnen Komponenten hergestellt und schließlich ein Prototyp mit der optimierten Kombination aufgebaut. Mit diesem Prototyp konnten die Ausgangsanforderungen erfolgreich validiert werden: Es wurde gezeigt, dass die Pumpe die gleichen geforderten Leistungswerte erreicht wie eine konventionelle Pumpe.

Im nächsten Schritt ging es darum, gezielt die spezifischen Vorteile der DE-Aktoren zu nutzen, um nicht nur den aktuellen Stand der Technik zu ersetzen, sondern auch einen technologischen Fortschritt zu erzielen. Dazu wurde zunächst eine kostengünstige Ansteuerungselektronik entwickelt, um auf teure Laborelektronik verzichten zu können.

Basierend auf dieser Elektronik wurde ein neuer Self-Sensing-Ansatz demonstriert, mit dem die druckabhängige maximale Amplitude durch die Analyse des Entladezyklus rekonstruiert werden kann. Diese Druckmessung mittels Self-Sensing ermöglicht es, die Pumpe autonom an veränderte Lastbedingungen anzupassen, indem die Ansteuerfrequenz so geregelt wird, dass die Pumpe stets im Resonanzbetrieb und damit energieoptimal arbeitet.

Für die Zukunft sind weitere Effizienzsteigerungen geplant. Konkret werden verschiedene Elektronikkonzepte untersucht, die es erlauben, einen Teil der beim Entladen der DE-Aktoren freiwerdenden Energie zurückzugewinnen. Ein vielversprechender Ansatz sieht vor, zwei Pumpkammern phasenversetzt um 180° anzusteuern. Dabei wird beim Entladen eines Aktors die Energie genutzt, um den anderen Aktor gleichzeitig aufzuladen. Vorteile dieses Verfahrens sind neben der Energierückgewinnung von bis zu 50 % auch eine Kompensation von Schwingungen, da die Kammern ähnlich wie bei einem Boxermotor angeordnet werden können.

Zusammenfassend lässt sich sagen, dass in dieser Dissertation anhand von zwei exemplarischen Anwendungsbeispielen aufgezeigt wurde, wie DE-Aktoren auf ein neues Leistungsniveau gebracht werden können, sowohl in komplexen Feldern wie der Softrobotik mit mehrdimensionalen Bewegungen als auch im Bereich dynamischer Anwendungen wie Pumpen. Dabei wurde stets das Gesamtsystem modellbasiert betrachtet und alle Einzelkomponenten sowie ihr Zusammenspiel optimiert. Die Leistungsfähigkeit der entwickelten Systeme konnte jeweils durch Prototypen eindrucksvoll demonstriert werden. Im Anschluss an die grundlegenden Leistungsnachweise wurden smarte Funktionen auf Basis von Self-Sensing integriert. Besonders bei der Pumpe führte dies zur Entwicklung eines Prototyps, der sich autonom und energieeffizient im Resonanzbetrieb regelt.

Übersicht der wissenschaftlichen Laufbahn

Journal Paper:

- Baltes, M. & Bruch, Daniel & Motzki, Paul. (2025). Model-Based Synchronization of Dielectric Elastomers and Membrane Pumps for Performance-Optimized, Space-Efficient, and Application-Specific Pump Design. Engineering Reports. 7. 10.1002/eng2.70237.
- Baltes, M., Holz, B., Bruch, D., & Motzki, P. (2025). Electronic Control System for Optimized Resonance Operation of Dielectric Elastomer Pumps through Self-Sensing. Advanced Engineering Materials. https://doi.org/10.1002/adem.202501204
- Baltes, Matthias & Kunze, Julian & Prechtl, Johannes & Seelecke, Stefan & Rizzello, Gianluca. (2022). A bi-stable soft robotic bendable module driven by silicone dielectric elastomer actuators: design, characterization, and parameter study. Smart Materials and Structures. 31. 10.1088/1361-665X/ac96df.
- Prechtl, Johannes & Baltes, Matthias & Flaßkamp, Kathrin & Rizzello, Gianluca. (2024). Sensorless Proprioception in Multi-DoF Dielectric Elastomer Soft Robots via System-Level Self-Sensing. IEEE/ASME Transactions on Mechatronics. PP. 10.1109/TMECH.2024.3375923.
- Soleti, Giovanni & Prechtl, Johannes & Massenio, Paolo & Baltes, Matthias & Rizzello, Gianluca. (2023). Energy based control of a bi-stable and underactuated soft robotic system based on dielectric elastomer actuators. IFAC-PapersOnLine. 56. 7796-7801. 10.1016/j.ifacol.2023.10.1153.

Konferenz Beiträge:

- Baltes, Matthias & Croce, Sipontina & Bruch, Daniel & Motzki, Paul. (2024). Resonance-Optimized Dielectric Pump Demonstrator With Self-Sensing Based Pressure Feedback. 10.1115/SMASIS2024-140331.
- Roth, Lukas & Croce, Sipontina & Baltes, Matthias & Nalbach, Sophie & Motzki, Paul. (2024). A Novel Tactile Feedback Wristband Based on a Dielectric Elastomer. 10.1115/SMASIS2024-140153.
- Baltes, Matthias & Bruch, Daniel & Seelecke, Stefan & Motzki, Paul. (2024). Resonance-optimized dielectric elastomer pump demonstrator: a dynamic systems approach. 3. 10.1117/12.3009967.
- Soleti, Giovanni & Prechtl, Johannes & Massenio, Paolo & Baltes, Matthias & Rizzello, Gianluca. (2023). Energy based control of a bi-stable and underactuated soft robotic system based on dielectric elastomer actuators.
- Matthias Baltes, Julian Kunze, Johannes Prechtl, Paul Motzki, Stefan Seelecke, Gianluca Rizzzello, "Soft robotic tentacle arm element actuated by rolled dielec-

tric elastomer artificial muscles," Proc. SPIE 12042, Electroactive Polymer Actuators and Devices (EAPAD) XXIV, 1204207 (20 April 2022); https://doi.org/10.1117/12.2612516

- M. Baltes, J. Prechtl, J. Kunze and G. Rizzello, "Design and Modeling of a Soft Robotic bendable module with Artificial Muscle Fibers," *ACTUATOR 2022; International Conference and Exhibition on New Actuator Systems and Applications*, Mannheim, Germany, 2022, pp. 1-4.
- EuroEap 2021:
  - 1.4.2 Modular pump design for DE based membrane pumps (Matthias Baltes, Sophie Nalbach, Gianluca Rizzello, Stefan Seelecke)
- EuroEap 2022:
  - 2.3.7 A bi-stable soft robotic bendable module driven by rolled DEAs: modeling, control, and self-sensing (Johannes Prechtl, Matthias Baltes, Julian Kunze, Paolo Roberto Massenio, Stefan Seelecke, Gianluca Rizzello)
  - 2.3.9 A bi-stable soft robotic bendable module driven by rolled deas: design, fabrication, and characterization (Julian Kunze, Matthias Baltes, Johannes Prechtl, Gianluca Rizzello, Stefan Seelecke)
- EuroEap 2023:
  - 1.3.1 A bi-stable soft robotic bendable module driven by silicone dielectric elastomer actuators: design, modeling, self-sensing, and position control (Giovanni Soleti, Johannes Prechtl, Matthias Baltes, Julian Kunze, Stefan Seelecke, Gianluca Rizzello)
- EuroEap 2024:
  - 2.2.14 Dynamic design approach for resonance optimized self-sense based dielectric elastomer pumps (Matthias Baltes, Sipontina Croce, Daniel Bruch, Sophie Nalbach, Paul Motzki)
  - 2.2.19 Novel haptic feedback armband based on dielectric-elastomers (Sipontina Croce, Lukas Roth, Matthias Baltes, Sophie Nalbach, Paul Motzki)

Hardware Challenges:

- EuroEAP 2021:
  2nd prize: App controlled, credit card sized DE-Actuator

- EuroEAP 2022:
  3rd prize: Dielectric Elastomer Rollercoaster

- SPIE 2024:
  EAP-in-action Demonstrator finalist: Resonance-optimized dielectric elastomer pump demonstrator

- SMASIS 2024:
  Wayne metals best hardware award second place: Resonance-optimized dielectric pump demonstrator with self-sense based pressure feedback

Literaturverzeichnis

[1] R. Bogue, “Smart materials: a review of capabilities and applications,” *Assembly Automation*, vol. 34, no. 1, pp. 16–22, Jan. 2014, doi: 10.1108/AA-10-2013-094.

[2] G. Song, N. Ma, and H.-N. Li, “Applications of shape memory alloys in civil structures,” *Eng Struct*, vol. 28, no. 9, pp. 1266–1274, Jul. 2006, doi: 10.1016/j.engstruct.2005.12.010.

[3] R. Britz and P. Motzki, “Analysis and evaluation of bundled SMA actuator wires,” *Sens Actuators A Phys*, vol. 333, p. 113233, Jan. 2022, doi: 10.1016/j.sna.2021.113233.

[4] F. Welsch, S.-M. Kirsch, P. Motzki, M. Schmidt, and S. Seelecke, “Vacuum Gripper System Based on Bistable SMA Actuation,” in *Volume 1: Development and Characterization of Multifunctional Materials; Modeling, Simulation, and Control of Adaptive Systems; Integrated System Design and Implementation*, American Society of Mechanical Engineers, Sep. 2018. doi: 10.1115/SMASIS2018-7980.

[5] X. Gao *et al.*, “Piezoelectric Actuators and Motors: Materials, Designs, and Applications,” *Adv Mater Technol*, vol. 5, no. 1, Jan. 2020, doi: 10.1002/admt.201900716.

[6] Y. Bar-Cohen and I. A. Anderson, “Electroactive polymer (EAP) actuators—background review,” *Mech Soft Mater*, vol. 1, no. 1, p. 5, Dec. 2019, doi: 10.1007/s42558-019-0005-1.

[7] *Dielectric Elastomers as Electromechanical Transducers*. Elsevier, 2008. doi: 10.1016/B978-0-08-047488-5.X0001-9.

[8] N. Ni and L. Zhang, “Dielectric Elastomer Sensors,” 2017. doi: 10.5772/intechopen.68995.

[9] J.-E. Potaufeux, J. Odent, D. Notta-Cuvier, F. Lauro, and J.-M. Raquez, “A comprehensive review of the structures and properties of ionic polymeric materials,” *Polym Chem*, vol. 11, no. 37, pp. 5914–5936, 2020, doi: 10.1039/D0PY00770F.

[10] S. Kirkman, P. Rothemund, E. Acome, and C. Keplinger, “Electromechanics of planar HASEL actuators,” *Extreme Mech Lett*, vol. 48, p. 101408, Oct. 2021, doi: 10.1016/j.eml.2021.101408.

[11] B. Fasolt, M. Hodgins, G. Rizzello, and S. Seelecke, “Effect of screen printing parameters on sensor and actuator performance of dielectric elastomer (DE) membranes,” *Sens Actuators A Phys*, vol. 265, pp. 10–19, Oct. 2017, doi: 10.1016/j.sna.2017.08.028.

[12] G. Rizzello, P. Serafino, D. Naso, and S. Seelecke, “Towards Sensorless Soft Robotics: Self-Sensing Stiffness Control of Dielectric Elastomer Actuators,” *IEEE Transactions on Robotics*, vol. 36, no. 1, pp. 174–188, 2020, doi: 10.1109/TRO.2019.2944592.

[13] J. Prechtl, M. Baltes, K. Flaßkamp, and G. Rizzello, “Sensorless Proprioception in Multi-DoF Dielectric Elastomer Soft Robots via System-Level Self-Sensing,” *IEEE/ASME Transactions on Mechatronics*, vol. 29, no. 6, pp. 4365–4376, Dec. 2024, doi: 10.1109/TMECH.2024.3375923.

[14] F. Beco Albuquerque and H. R. Shea, “Effect of humidity, temperature, and elastomer material on the lifetime of silicone-based dielectric elastomer actuators under a constant DC electric field (Conference Presentation),” in *Electroactive Polymer Actuators and Devices (EAPAD) XXII*, Y. Bar-Cohen, I. A. Anderson, and H. R. Shea, Eds., SPIE, Apr. 2020, p. 42. doi: 10.1117/12.2558428.

[15] S. Michel, X. Zhang, M. Wissler, C. Löwe, and G. Kovacs, “A comparison between silicone and acrylic elastomers as dielectric materials in electroactive polymer actuators,” *Polym Int*, vol. 59, pp. 391–399, Mar. 2009, doi: 10.1002/pi.2751.

[16] Y. Chen, L. Agostini, G. Moretti, M. Fontana, and R. Vertechy, “Dielectric elastomer materials for large-strain actuation and energy harvesting: a comparison between styrenic rubber, natural rubber and acrylic elastomer,” *Smart Mater Struct*, vol. 28, no. 11, p. 114001, Oct. 2019, doi: 10.1088/1361-665x/ab3b32.

[17] M. Han, J. Lee, J. K. Kim, H. K. An, S.-W. Kang, and D. Jung, “Highly sensitive and flexible wearable pressure sensor with dielectric elastomer and carbon nanotube electrodes,” *Sens Actuators A Phys*, vol. 305, p. 111941, Apr. 2020, doi: 10.1016/j.sna.2020.111941.

[18] J. Hubertus, S. Croce, J. Neu, S. Seelecke, G. Rizzello, and G. Schultes, “Laser Structuring of Thin Metal Films of Compliant Electrodes on Dielectric Elastomers,” *Adv Funct Mater*, vol. 33, no. 16, Apr. 2023, doi: 10.1002/adfm.202214176.

[19] S. Rosset and H. R. Shea, “Flexible and stretchable electrodes for dielectric elastomer actuators,” *Applied Physics A*, vol. 110, no. 2, pp. 281–307, Feb. 2013, doi: 10.1007/s00339-012-7402-8.

[20] E. Hajiesmaili and D. R. Clarke, “Dielectric elastomer actuators,” *J Appl Phys*, vol. 129, no. 15, p. 151102, Apr. 2021, doi: 10.1063/5.0043959.

[21] S. Gratz-Kelly, T. F. Krüger, S. Seelecke, G. Rizzello, and G. Moretti, “A tri-modal dielectric elastomer actuator integrating linear actuation, sound generation, and self-sensing capabilities,” *Sens Actuators A Phys*, vol. 372, p. 115332, Jul. 2024, doi: 10.1016/j.sna.2024.115332.

[22] G. Kovacs, L. Düring, S. Michel, and G. Terrasi, "Stacked dielectric elastomer actuator for tensile force transmission," *Sens Actuators A Phys*, vol. 155, no. 2, pp. 299–307, 2009, doi: https://doi.org/10.1016/j.sna.2009.08.027.

[23] S. Hau, A. York, G. Rizzello, and S. Seelecke, "Performance Prediction and Scaling Laws of Circular Dielectric Elastomer Membrane Actuators," *Journal of Mechanical Design*, vol. 140, no. 11, Nov. 2018, doi: 10.1115/1.4039104.

[24] M. Hodgins and S. Seelecke, "Mechanical Behavior of a Bi-Stable Negative-Rate Bias Spring System," *Proceedings of SPIE - The International Society for Optical Engineering*, vol. 7644, Mar. 2010, doi: 10.1117/12.852373.

[25] P. Loew, G. Rizzello, and S. Seelecke, "A Novel Biasing Mechanism for Circular out-of-plane Dielectric Actuators Based on Permanent Magnets," *Mechatronics*, vol. 56, pp. 48–57, Oct. 2018, doi: 10.1016/j.mechatronics.2018.10.005.

[26] M. Hodgins and S. Seelecke, "Experimental Analysis of Biasing Elements for Dielectric Electro-Active Polymers," *Proceedings of SPIE - The International Society for Optical Engineering*, vol. 7976, Oct. 2011, doi: 10.1117/12.883555.

[27] J. Neu, J. Hubertus, S. Croce, G. Schultes, S. Seelecke, and G. Rizzello, "Fully Polymeric Domes as High-Stroke Biasing System for Soft Dielectric Elastomer Actuators," *Front Robot AI*, vol. 8, p. 171, 2021, doi: 10.3389/frobt.2021.695918.

[28] S. Hau, D. Bruch, G. Rizzello, P. Motzki, and S. Seelecke, "Silicone based dielectric elastomer strip actuators coupled with nonlinear biasing elements for large actuation strains," *Smart Mater Struct*, vol. 27, no. 7, p. 74003, Jun. 2018, doi: 10.1088/1361-665x/aab7d8.

[29] M. Hodgins, A. York, and S. Seelecke, "Experimental comparison of bias elements for out-of-plane DEAP actuator system," *Smart Mater Struct*, vol. 22, no. 9, p. 094016, 2013, doi: 10.1088/0964-1726/22/9/094016.

[30] M. Giousouf and G. Kovacs, "Dielectric elastomer actuators used for pneumatic valve technology," *Smart Mater Struct*, vol. 22, no. 10, p. 104010, Oct. 2013, doi: 10.1088/0964-1726/22/10/104010.

[31] M. Hill, G. Rizzello, and S. Seelecke, "Development and experimental characterization of a pneumatic valve actuated by a dielectric elastomer membrane," *Smart Mater Struct*, vol. 26, no. 8, p. 085023, Aug. 2017, doi: 10.1088/1361-665X/aa746d.

[32] S. Wei and T. K. Ghosh, "Bioinspired Bistable Dielectric Elastomer Actuators: Programmable Shapes and Application as Binary Valves," *Soft Robot*, vol. 9, no. 5, pp. 900–906, Oct. 2022, doi: 10.1089/soro.2020.0214.

[33] K. Flittner, M. Schlosser, and H. F. Schlaak, “Dielectric elastomer stack actuators for integrated gas valves,” Y. Bar-Cohen and F. Carpi, Eds., Mar. 2011, p. 79761K. doi: 10.1117/12.880050.

[34] Y. Goergen *et al.*, “Shape Memory Alloys in Continuum and Soft Robotic Applications,” in *ASME 2019 Conference on Smart Materials, Adaptive Structures and Intelligent Systems*, American Society of Mechanical Engineers, Sep. 2019. doi: 10.1115/SMASIS2019-5610.

[35] Y. Nakabo, T. Mukai, and K. Asaka, “Biomimetic Soft Robots Using IPMC,” in *Electroactive Polymers for Robotic Applications*, London: Springer London, pp. 165–198. doi: 10.1007/978-1-84628-372-7_7.

[36] F. Schmitt, O. Piccin, L. Barbé, and B. Bayle, “Soft Robots Manufacturing: A Review,” *Front Robot AI*, vol. 5, 2018, doi: 10.3389/frobt.2018.00084.

[37] D. Rus and M. T. Tolley, “Design, fabrication and control of soft robots,” *Nature*, vol. 521, no. 7553, pp. 467–475, 2015, doi: 10.1038/nature14543.

[38] G.-Y. Gu, J. Zhu, L.-M. Zhu, and X. Zhu, “A survey on dielectric elastomer actuators for soft robots,” *Bioinspiration &amp Biomimetics*, vol. 12, no. 1, p. 11003, Jan. 2017, doi: 10.1088/1748-3190/12/1/011003.

[39] J. Shintake, V. Cacucciolo, H. Shea, and D. Floreano, “Soft Biomimetic Fish Robot Made of Dielectric Elastomer Actuators,” *Soft Robot*, vol. 5, no. 4, pp. 466–474, 2018, doi: 10.1089/soro.2017.0062.

[40] Z. Xing, J. Zhang, D. McCoul, Y. Cui, L. Sun, and J. Zhao, “A Super-Lightweight and Soft Manipulator Driven by Dielectric Elastomers.,” *Soft Robot*, vol. 7, no. 4, Aug. 2020, doi: 10.1089/soro.2018.0134.

[41] U. Gupta, L. Qin, Y. Wang, H. Godaba, and J. Zhu, “Soft robots based on dielectric elastomer actuators: a review,” *Smart Mater Struct*, vol. 28, no. 10, p. 103002, Sep. 2019, doi: 10.1088/1361-665x/ab3a77.

[42] H. Godaba, J. Li, Y. Wang, and J. Zhu, “A Soft Jellyfish Robot Driven by a Dielectric Elastomer Actuator,” *IEEE Robot Autom Lett*, vol. 1, no. 2, pp. 624–631, 2016, doi: 10.1109/LRA.2016.2522498.

[43] J. Zhao, J. Zhang, D. McCoul, Y. Cui, and X. Lan, “A Soft Biomimetic Module of Elephant Trunk Driven by Dielectric Elastomers,” in *2018 IEEE International Conference on Robotics and Biomimetics (ROBIO)*, 2018, pp. 349–354. doi: 10.1109/ROBIO.2018.8665147.

[44] E. Rustighi, W. Kaal, S. Herold, and A. Kubbara, “Experimental Characterisation of a Flat Dielectric Elastomer Loudspeaker,” *Actuators*, vol. 7, no. 2, p. 28, Jun. 2018, doi: 10.3390/act7020028.

[45] G. Moretti, G. Rizzello, M. Fontana, and S. Seelecke, “A multi-domain dynamical model for cone-shaped dielectric elastomer loudspeakers,” in *Electroactive Polymer Actuators and Devices (EAPAD) XXIII*, J. D. Madden, I. A. Anderson, and H. R. Shea, Eds., SPIE, Mar. 2021, p. 53. doi: 10.1117/12.2581718.

[46] L. Roth, S. Croce, M. Baltes, S. Nalbach, and P. Motzki, “A Novel Tactile Feedback Wristband Based on a Dielectric Elastomer,” in *ASME 2024 Conference on Smart Materials, Adaptive Structures and Intelligent Systems*, American Society of Mechanical Engineers, Sep. 2024. doi: 10.1115/SMASIS2024-140153.

[47] M. Smith, V. Cacucciolo, and H. Shea, “Fiber pumps for wearable fluidic systems,” *Science (1979)*, vol. 379, no. 6639, pp. 1327–1332, Mar. 2023, doi: 10.1126/science.ade8654.

[48] N. Goulbourne, M. I. Frecker, E. M. Mockensturm, and A. J. Snyder, “Modeling of a dielectric elastomer diaphragm for a prosthetic blood pump,” in *Smart Structures and Materials 2003: Electroactive Polymer Actuators and Devices (EAPAD)*, Y. Bar-Cohen, Ed., SPIE, 2003, pp. 319 – 331. doi: 10.1117/12.484388.

[49] P. Linnebach, G. Rizzello, and S. Seelecke, “Design and Validation of a Dielectric Elastomer Membrane Actuator Driven Pneumatic Pump,” *Smart Mater Struct*, vol. 29, Apr. 2020, doi: 10.1088/1361-665X/ab8a01.

[50] A. Kumar, D. Ahmad, and K. Patra, *Electromechanical Characterization of Dielectric Elastomer Actuator based Pump for Optimum Volume Flow Rate*. 2018.

[51] G. Mao *et al.*, “Design and Characterization of a Soft Dielectric Elastomer Peristaltic Pump Driven by Electromechanical Load,” *IEEE/ASME Transactions on Mechatronics*, vol. 23, no. 5, pp. 2132–2143, 2018, doi: 10.1109/TMECH.2018.2864252.

[52] J. Chavanne *et al.*, “Manufacturing and Tests of a Tubular Multilayer Dielectric Elastomer Actuator for an Impedance Pump,” in *2020 23rd International Conference on Electrical Machines and Systems (ICEMS)*, IEEE, Nov. 2020, pp. 380–383. doi: 10.23919/ICEMS50442.2020.9290904.

[53] G. Mao *et al.*, “Design and Characterization of a Soft Dielectric Elastomer Peristaltic Pump Driven by Electromechanical Load,” *IEEE/ASME Transactions on Mechatronics*, vol. 23, no. 5, pp. 2132–2143, 2018, doi: 10.1109/TMECH.2018.2864252.

[54] S. Ho *et al.*, “Experimental characterization of a dielectric elastomer fluid pump and optimizing performance via composite materials,” *J Intell Mater Syst Struct*, vol. 28, no. 20, pp. 3054–3065, Dec. 2017, doi: 10.1177/1045389X17704921.

[55] Y. Wang, Z. Li, L. Qin, G. Caddy, C. H. Yap, and J. Zhu, “Dielectric Elastomer Fluid Pump of High Pressure and Large Volume Via Synergistic Snap-Through,” *J Appl Mech*, vol. 85, no. 10, Oct. 2018, doi: 10.1115/1.4040478.

[56] G. Soleti, P. R. Massenio, J. Kunze, and G. Rizzello, “Model-Based Robust Position Control of an Underactuated Dielectric Elastomer Soft Robot,” *IEEE Transactions on Robotics*, vol. 41, pp. 1693–1710, 2025, doi: 10.1109/TRO.2025.3539184.

[57] G. Soleti, J. Prechtl, P. R. Massenio, M. Baltes, and G. Rizzello, “Energy based control of a bi-stable and underactuated soft robotic system based on dielectric elastomer actuators*,” *IFAC-PapersOnLine*, vol. 56, no. 2, pp. 7796–7801, 2023, doi: 10.1016/j.ifacol.2023.10.1153.

Beitragsberichte zu den eingebundenen Publikationen

Im Rahmen dieser Dissertation wurden mehrere wissenschaftliche Beiträge verfasst, von denen ein Teil bereits veröffentlicht oder zur Publikation eingereicht wurde. Die folgenden Tabellen geben einen Überblick über die eingebundenen Publikationen, den jeweiligen Beitrag der Autorin/des Autors, den Status der Beiträge sowie Informationen zur Art der Begutachtung und zur wissenschaftlichen Qualität der Veröffentlichungsorgane.

A bi-stable soft robotic bendable module driven by silicone dielectric elastomer actuators: design, characterization, and parameter study

Journal:	Smart Materials and Structures
Verlag:	IOP Publishing
Qualität:	Forschungsartikel
Status:	Veröffentlicht am 17. Oktober 2022 nach Peer-Review Begutachtung.

Matthias Baltes war verantwortlich für die Planung und Durchführung der Versuchsreihen sowie der Messungen. Zudem entwickelte, designte und fertigte er den Prototyp und konzipierte den Prüfstand zur Charakterisierung. Darüber hinaus validierte er das Modell und erstellte das Manuskript einschließlich der Abbildungen.

Julian Kunze war verantwortlich für die Entwicklung des Herstellungsverfahren und die Herstellung der gerollten dielektrischen Elastomer Aktoren (RDEAs), welche in dieser Arbeit verwendet wurden.

Johannes Prechtl war verantwortlich für die theoretische Analyse der Grundstruktur, deren mathematische Betrachtung und Entwicklung eines entsprechenden Modells.

Stefan Seelecke war in beratender Funktion tätig.

Gianluca Rizzello hat das Manuskript Korrektur gelesen und war in beratender Funktion tätig.

Matthias Baltes

Julian Kunze   Johannes Prechtl   Stefan Seelecke   Gianluca Rizello

Model-Based Synchronization of Dielectric Elastomers and Membrane Pumps for Performance-Optimized, Space-Efficient, and Application-Specific Pump Design.

Journal: Engineering Reports

Verlag: Wiley

Qualität: Forschungsartikel

Status: Veröffentlicht am 16. Juni 2025 nach Peer-Review Begutachtung.

Matthias Baltes war verantwortlich für die Entwicklung des Modells, den Aufbau und die Validierung der einzelnen Komponenten sowie die Konzeption und den Aufbau des Prüfstands zur Systemvalidierung. Zudem plante und führte er die Messungen durch, war für das Design und den Bau des Gesamtsystems einschließlich dessen Validierung zuständig und verfasste das Manuskript einschließlich der Abbildungen.

Daniel Bruch hat das Manuskript Korrektur gelesen und war in beratender Funktion tätig.

Paul Motzki hat das Manuskript Korrektur gelesen und war in beratender Funktion tätig.

Matthias Baltes

Daniel Bruch

Paul Motzki

Electronic Control System for Optimized Resonance Operation of Dielectric Elastomer Pumps Through Self-Sensing

Journal: Advanced Engineering Materials

Verlag: Wiley

Qualität: Forschungsartikel

Status: Veröffentlicht am 1. Juli 2025 nach Peer-Review Begutachtung.

Matthias Baltes entwickelte die Grundidee des Konzepts zur Self-Sensing-Erfassung des Pumpendrucks. Er führte Validierungsmessungen zum Proof-of-Concept an der Pumpe durch, wertete die Messdaten aus und entwickelte das zugehörige Ansteuerungskonzept. Zudem verfasste er das Manuskript einschließlich der Abbildungen.

Benedikt Holz war verantwortlich für die Entwicklung des Hochspannungselektronikkonzepts sowie den Aufbau der entsprechenden Elektronik. Zudem führte er Messungen und Validierungen am realen Pumpenprototyp durch und verfasste die entsprechenden Abschnitte des Manuskripts.

Daniel Bruch hat das Manuskript Korrektur gelesen und war in beratender Funktion tätig.

Paul Motzki hat das Manuskript Korrektur gelesen und war in beratender Funktion tätig.

Matthias Baltes

Benedikt Holz

Daniel Bruch

Paul Motzki